Chemical Geology 636 (2023) 121630

Contents lists available at ScienceDirect

Chemical Geology

journal homepage: www.elsevier.com/locate/chemgeo

Apatite laser ablation Lu—Hf geochronology: A new tool to date mafic rocks

Melissa B.K. Kharkongor [a,*], Stijn Glorie [a], Jacob Mulder [a], Christopher L. Kirkland [b], David Chew [c], Barry Kohn [d], Alexander Simpson [a]

[a] Department of Earth Sciences, University of Adelaide, SA 5005, Australia
[b] Timescales of Mineral Systems Group, School of Earth and Planetary Sciences, Curtin University, WA 6102, Australia
[c] Department of Geology, Trinity College Dublin, The University of Dublin, Dublin 2, Ireland
[d] School of Geography, Earth and Atmospheric Sciences, University of Melbourne, Melbourne, Victoria 3010, Australia

ARTICLE INFO

Editor: Claudia Romano

Keywords:
Mafic rocks
apatite
U–Pb dating
Lu—Hf dating
LA-ICP-MS/MS
Closure temperature
recrystallisation

ABSTRACT

Mafic rocks are the most common type of igneous rocks on Earth, however, constraining the crystallization age of mafic rocks can be challenging. Apatite is a common accessory phase in mafic rocks and is amenable to dating using the U–Pb system. However, the U–Pb system in apatite has a relatively low closure temperature (~350°-550 °C) and is therefore prone to resetting by later thermal and metasomatic events. Here, a recently developed Lu—Hf dating method using laser ablation reaction-cell mass spectrometry is applied to apatite from mafic rocks. The Lu—Hf system in apatite has a higher closure temperature (~650°-750 °C) compared to U–Pb, increasing the chances of obtaining primary crystallization ages. Furthermore, the laser-ablation method allows rapid data collection compared to traditional solution-based Lu—Hf dating techniques. Four study areas were selected to compare the Lu—Hf vs U–Pb systematics of apatite in mafic igneous rocks: the Paleoproterozoic Sudbury Igneous Complex (Canada), the Neoproterozoic Borborema Province (NE Brazil), the Paleoproterozoic Fennoscandian Shield (Finland), the Archean Yilgarn Craton and adjacent Mesoproterozoic Albany Fraser Orogen (Western Australia). For all analyzed samples that have apatite trace element compositions typical of an undisturbed primary mafic igneous lithology, the Lu—Hf system retains primary igneous apatite crystallization ages, whereas the U–Pb system in the same grains often records isotopic disturbance or a cooling age. In few cases, the Lu—Hf system has also been disturbed in response to recrystallization, however, such disturbance is readily detected with trace element data. Hence, this study demonstrates the potential of laser ablation apatite Lu—Hf dating to obtain primary crystallization ages for otherwise difficult to date mafic rocks.

1. Introduction

Solid Earth geochronology, particularly for felsic magmatic and metamorphic rocks, has largely focused on the U–Pb systematics of the mineral zircon ($ZrSiO_4$), for several reasons: (1) The U–Pb zircon system exploits two independent decay schemes, ^{235}U to ^{207}Pb and ^{238}U to ^{206}Pb; (2) the U–Pb zircon system is often unaffected by post-crystallization alteration and U–Pb system disturbances; (3) it has a high closure temperature for Pb diffusion (>900 °C); and (4) typically has high radiogenic to initial Pb ratios allowing precise dating (e.g., Gehrels, 2011; Puetz and Spencer, 2023; Puetz et al., 2021). However, dating mafic rocks with zircons is more challenging because zircon generally has low fertility in mafic lithologies (Jennings et al., 2011; Boehnke et al., 2013). Zr-rich mafic melts may instead crystallise baddeleyite (ZrO_2) or zirconolite ($CaZrTiO_2O_7$), which are also amenable to U–Pb dating (e.g., Söderlund et al., 2010) but are commonly too small to be analysed using in situ techniques, and in the case of baddeleyite, have significant crystal orientation effects when analysed via ion beam methods (Wingate and Compston, 2000). Alternatively, mafic rocks can be dated by the $^{40}Ar—^{39}Ar$ method applied to plagioclase or pyroxene (Ware and Jourdan, 2018), however age interpretations can be challenging, especially for old rocks with significant degrees of alteration (Jiang et al., 2021).

Apatite is a common accessory phase in many igneous lithologies (e.g. Piccoli and Candela, 2002;Chew and Spikings, 2015), including pegmatites, cumulates (Ihlen et al., 2014), and carbonatites (McArthur,

* Corresponding author at: Department of Earth Sciences, University of Adelaide, Adelaide, SA 5005, Australia.
E-mail address: melissa.kharkongor@adelaide.edu.au (M.B.K. Kharkongor).

https://doi.org/10.1016/j.chemgeo.2023.121630
Received 14 April 2023; Received in revised form 28 June 2023; Accepted 8 July 2023
Available online 13 July 2023

1985). Unlike most other U-bearing accessory phases, apatite is common in (ultra-)mafic rocks (Spear and Pyle, 2002; Piccoli and Candela, 2002; Webster and Piccoli, 2015). Apatite also grows in metamorphic rocks, including those with mafic protoliths, and is found at all metamorphic grades from diagenetic environments to migmatites (Spear and Pyle, 2002). Several studies have applied apatite U–Pb dating to constrain the age of (ultra-)mafic rocks (O'Sullivan et al., 2016; Pochon et al., 2016; Gillespie et al., 2018; Ackerman et al., 2020). However, apatite U–Pb dating can be challenging since apatite commonly incorporates a significant component of non-radiogenic (initial) Pb in its crystal lattice (Kirkland et al., 2018). Moreover, apatite in mafic rocks tends to have low U concentrations, resulting in a low ratio of radiogenic Pb to initial Pb, which results in increased age uncertainty. Additionally, the closure temperature of Pb diffusion in apatite is significantly lower (~350—570 °C; Chew and Spikings, 2015) compared to zircon (~900 °C; Lee et al., 1997). Hence, the U–Pb isotopic system in apatite is susceptible to being reset by post-crystallization thermal events (Kirkland et al., 2018; Glorie et al., 2019; Henrichs et al., 2019). Thus, the apatite U–Pb system may not record primary igneous or metamorphic crystallization ages.

The Lu—Hf system in apatite has a significantly higher closure temperature (~ 660—730 °C; Cherniak, 2000; Barfod et al., 2005; Glorie et al., 2023) than the U–Pb system, making it less prone to post-crystallization resetting. For example, Glorie et al. (2022, 2023) demonstrated that Lu—Hf ages can be preserved in apatite grains that have experienced up to upper amphibolite-facies metamorphism, during which the U–Pb system was partially or completely reset in the same grains. Furthermore, Gillespie et al. (2022) showed apatite Lu—Hf ages to be similar to Sm—Nd ages for the same samples, consistent with the similar closure temperature of these two isotopic systems. Traditional apatite Lu—Hf dating involves sample digestion and addition of an isotope tracer, followed by chemical separation of Lu and Hf and analysis by MC-ICP-MS to obtain precise apatite crystallization ages (e.g., Larsson and Söderlund, 2005; Barfod et al., 2002; Barfod et al., 2003). However, the method is time-consuming, and due to the low Hf concentration in apatite, large aliquots are required (~0.5 g; Barfod et al., 2003). Hence, spatially resolved isotope ratios cannot easily be obtained (Schmidt et al., 2015). In contrast, the recent development of in situ (laser-ablation based) Lu—Hf geochronology (Simpson et al., 2021) provides an alternative and more rapid means of dating using the Lu—Hf system, which requires minimal sample preparation, has spatial resolution sufficient to resolve geological complexity (~60—100 μm), and preserves the textural context of the analysed mineral grains. This method uses NH_3 gas in the reaction cell of the LA-ICP-MS/MS (laser ablation tandem inductively coupled mass spectrometer) to chemically separate ^{176}Lu from ^{176}Hf, allowing both isotopes to be measured free from isobaric interferences. A detailed description of the method is provided in Simpson et al. (2021).

This study presents the first systematic evaluation of Lu—Hf dating of apatite via LA-ICP-MS/MS for determining the magmatic crystallization age of mafic (meta-)igneous rocks. Lu—Hf ages, U–Pb ages, and trace element data are integrated in apatite from mafic igneous rocks spanning near-pristine intrusions through to strongly deformed and metamorphosed meta-igneous rocks. Case studies from four different geological settings highlight that the Lu—Hf system in apatite generally preserves primary igneous crystallization ages, even in metamorphic rocks in which the U–Pb system in apatite has been thermally reset. Furthermore, trace element data from apatite allows filtering of those cases in which the Lu—Hf system is disturbed, primarily as a result of recrystallization of apatite grains. These findings demonstrate that Lu—Hf dating of apatite by LA-ICP-MS/MS proves a powerful new tool in the quest to rapidly, accurately, and routinely date mafic igneous rocks.

2. Geological background and sample descriptions

A total of twelve samples of mafic (meta-)igneous rocks were selected from four geological terranes that have experienced different degrees of thermal overprinting and/or deformation, which could potentially disturb the isotopic systematics of apatite. In order of increasing degree of thermal overprinting, these study areas include: (1) the Sudbury Igneous Complex in the Superior Craton, Canada; (2) the Borborema Province, NE Brazil; (3) the Fennoscandian Shield, Finland; (4) the Yilgarn Craton and Albany Fraser Orogen, Western Australia.

2.1. Sudbury Igneous Complex, Canada

The Sudbury Igneous Structure is located in the southern Canadian Shield at the boundary between the Archean Superior Province and the Mesoproterozoic Grenville Orogen (Fig. 1). The structure is divided into two broad units: (1) country rocks that form the footwall of the Sudbury Basin and (2) rock units within the Sudbury Basin, which include the Sudbury Igneous Complex (SIC) and the Whitewater Group (i.e. the Onwatin and Onaping Formations; Fig. 1). The Sudbury Igneous Complex (SIC) is generally interpreted to represent a differentiated impact melt sheet located within the Sudbury Structure (Lightfoot et al., 1997; Lightfoot and Doherty, 2001; Therriault et al., 2002). Detailed descriptions of the geological setting can be found in Dressler et al. (1984), Dessureau (2003), Lorencak et al. (2004) and Petrus et al., (2015). The SIC is subdivided into a discontinuous sub-layer and the main mass (Naldrett et al., 1970; Grieve et al., 1994; Lorencak et al., 2004). The discontinuous sublayer consists of mafic and ultramafic rocks, which locally host economically significant Ni—Cu deposits (Dressler et al., 1984; Dickin et al., 1992; Lightfoot et al., 1997). The main mass comprises a variable assemblage of granophyre, quartz gabbro and norite overlying the strongly brecciated footwall rocks in the basal contact zone of the structure (Dressler et al., 1984; Grieve et al., 1994). The southern part of the structure is affected by northwest-directed thrust faulting, resulting in the present-day elliptical shape of the Sudbury Basin (Milkereit and Green, 1992) (Fig. 1). A greenschist-facies metamorphic overprint is recorded in rocks in the south of the structure and decreases towards the north (Dietz, 1964; Grieve et al., 1994). The north of the structure is mostly undeformed with a weak sub-greenschist-facies metamorphic overprint (Lorencak et al., 2004; Milkereit and Green, 1992).

Three samples were taken from a 3400-m-deep drill hole from the northwest range of the SIC (Fig. 1), including a quartz gabbro from 2006 m (00ML11), a norite from 2298 m (00ML13) and a gabbro from 3447 m (00ML19). Sample 00ML11 is a quartz gabbro consisting of cumulus plagioclase and augite, with 10% cumulus oxides, 8% cumulus apatite, and intercumulus clinopyroxene, quartz, and feldspar intergrowths (Dressler et al., 1984; Dessureau, 2003). Sample 00ML13 is a norite from the lowest unit of the main mass in the North Range. It contains 40—60% hypersthene enclosed in large plagioclase, cumulus orthopyroxene as the only cumulus mineral, with <10% quartz with K-feldspar intergrowths, <10% biotite and < 10% clinopyroxene (Dressler et al., 1984; Dessureau, 2003). Sample 00ML19 is a gabbro from the footwall breccia, which is heterolithic, composed of angular to subrounded fragments and granoblastic quartz-feldspar intergrowths with plagioclase crystals (Dressler et al., 1984).

Concordant U–Pb zircon and baddeleyite ages of 1850 ± 3.4 Ma, 1850 ± 3 Ma and 1849 ± 1 Ma (Krogh et al., 1984) were obtained respectively from a mafic norite, granophyre, and norite within the main mass of the SIC near the sampled drillhole and are interpreted as constraining the crystallization age of the struture, providing a reference age for this case study. Deformation and greenschist metamorphism are inferred to have occurred after emplacement of the structure, during the ~1800–1820 Ma Penokean Orogeny (Fleet et al., 1987). Deformation during the ~1000 Ma Grenville Orogeny is thought to have had a minimal effect on the Sudbury Basin as Grenvillian metamorphism of

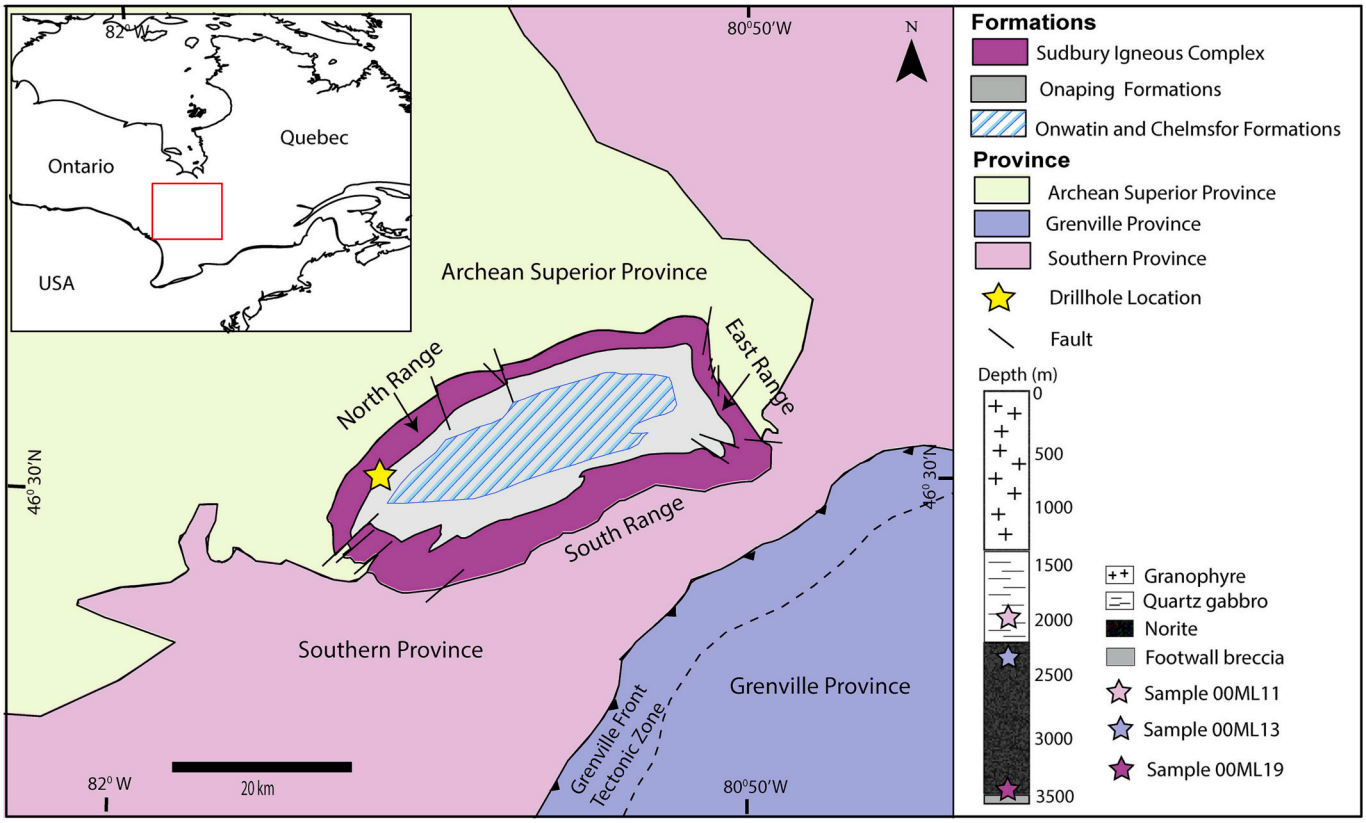

Fig. 1. Location map for the samples in the Sudbury Igneous Complex, Canada. Map modified from Lorencak et al. (2004) and Clark and Riller, (2018). The black star with yellow outline shows the drillhole location. (For interpretation of the references to colour in this figure legend, the reader is referred to the web version of this article.)

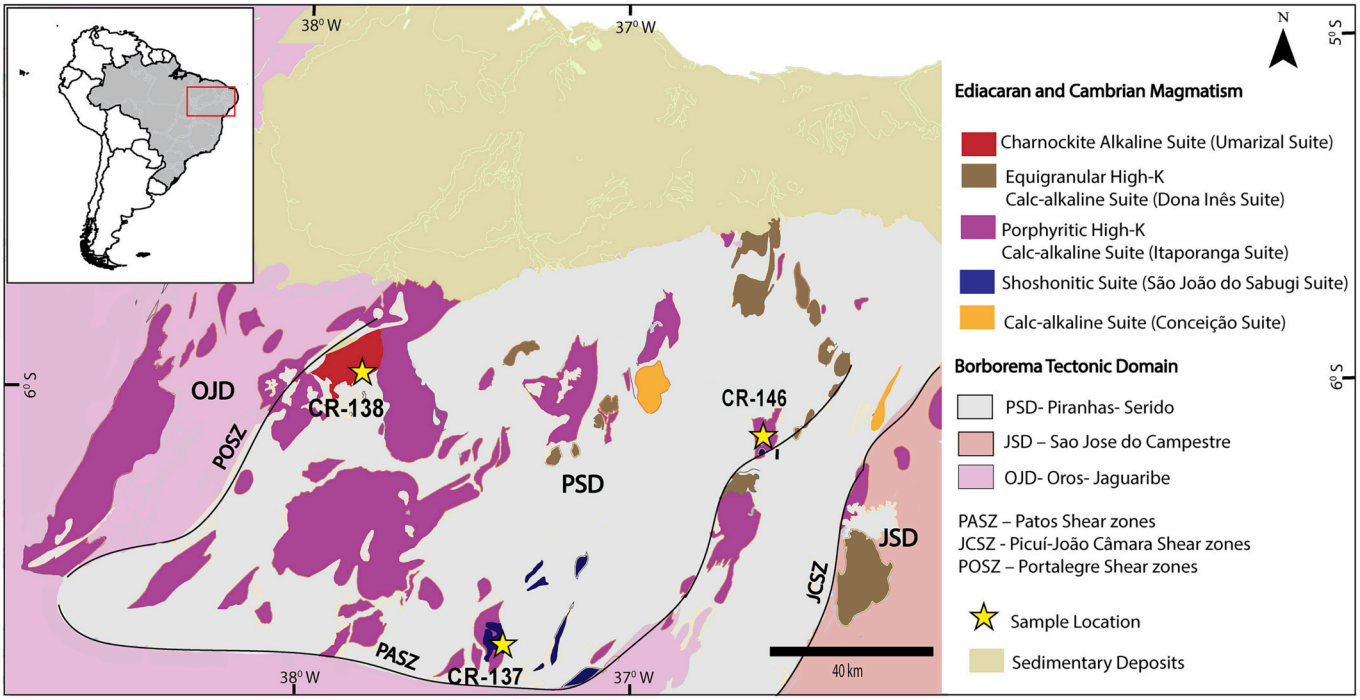

Fig. 2. Location map of the samples taken from Neoproterozoic intrusions within the Piranhas-Seridó Domain (PSD), a segment of the Borborema Province, NE Brazil. Map modified from Aragão et al. (2020) and the location of the different suites was adapted from Nascimento et al. (2015). Star symbols show the sample locations.

the regional Sudbury dyke swarm is restricted to within a few kilometres of the Grenville front to the south (Bethune and Davidson, 1997).

2.2. Borborema Province, NE Brazil

Apatite grains were obtained from Neoprotorozoic mafic intrusions (leucogabbro and leuconorite) associated with the Brasiliano orogenic event in Borborema Province, NE Brazil (Almeida et al., 1977; Caxito et al., 2020; Neves et al., 2014; De Almeida et al., 1981). The Borborema Province is composed of Archaean – Palaeoproterozoic crustal blocks, separated by crustal-scale shear zones, and is subdivided into the northern, southern, and central sub-provinces (Van Schmus et al., 1995). Samples were selected from the Piranhas-Seridó Domain (PSD), which is a segment of the northern sub-province of the Borborema Province (Fig. 2). The PSD is bounded to the north by Phanerozoic sedimentary rocks of the Coastal Province and the Potiguar Basin; and to the east, south, and west by the Portalegre, Picuí- João-Câmara, and Patos shear zones, respectively (Neves, 2003; Dantas, 2017; Medeiros et al., 2021).

The PSD was affected by extensive Ediacaran —Cambrian plutonic activity, producing six compositionally distinct magmatic suites, ranging from shoshonitic to alkaline charnockites (Nascimento et al., 2015) (Fig. 2). Sample CR-137 and Sample CR-146 were sampled from the São João do Sabugi shoshonitic Suite, which is composed of pyroxene-biotite gabbros and diorites and have a fine to medium equigranular texture with plagioclase phenocrysts. The mineralogy of the least evolved rocks comprises augite, diopside (locally replaced by amphibole), and in more differentiated lithologies (diorite/ quartz monzonite) consists mostly of hornblende and biotite; with titanite, zircon, and apatite as accessory minerals (Nascimento et al., 2015). The diorites were emplaced at 579 ± 7 Ma as determined by U–Pb ages from magmatic zircon grains (Leterrier et al., 1994). However, nearby gabbronorite samples from the same shoshonitic suite (Poço Verde and Totoró) yield slightly older zircon U–Pb crystallization ages of 599 ± 16 Ma and 595 ± 3 Ma (Archanjo et al., 2013). Additionally, monazite U–Pb ages of 553 ± 10 Ma from the same gabbronorite, indicate that a thermal event (potentially up to granulite facies) affected this Suite (Souza de et al., 2006).

Sample CR-138 was collected from gabbro-norite stocks associated with the Umarizal pluton, and is composed of fayalite, hedenbergite, hornblende and biotite, with zircon, allanite, titanite, magnetite, and apatite as accessory minerals (Galindo et al., 1995). Zircon U–Pb ages of 593 ± 5 Ma and 601 ± 11 Ma have been obtained for the Umarizal pluton (McReath et al., 2002; Sá et al., 2013). Additionally, a zircon U–Pb age of 581 ± 4 Ma was obtained from migmatized hornfels in the contact aureole of the Umarizal pluton, which is interpreted to date high-temperature (~ 700–800 °C) contact metamorphism of the country rocks (Nascimento Souza and Oliveira, 2022). A Rb—Sr age of 545 ± 7 Ma for the Umarizal pluton (Galindo, 1993), suggests a protracted cooling history following pluton emplacement and contact metamorphism.

2.3. Fennoscandian Shield, Finland

Samples were obtained from mafic intrusions in the Raahe-Ladoga zone in Central Finland (Fig. 3). This area represents a series of crustal blocks, separated by NW-SE trending shear zones and strike-slip faults

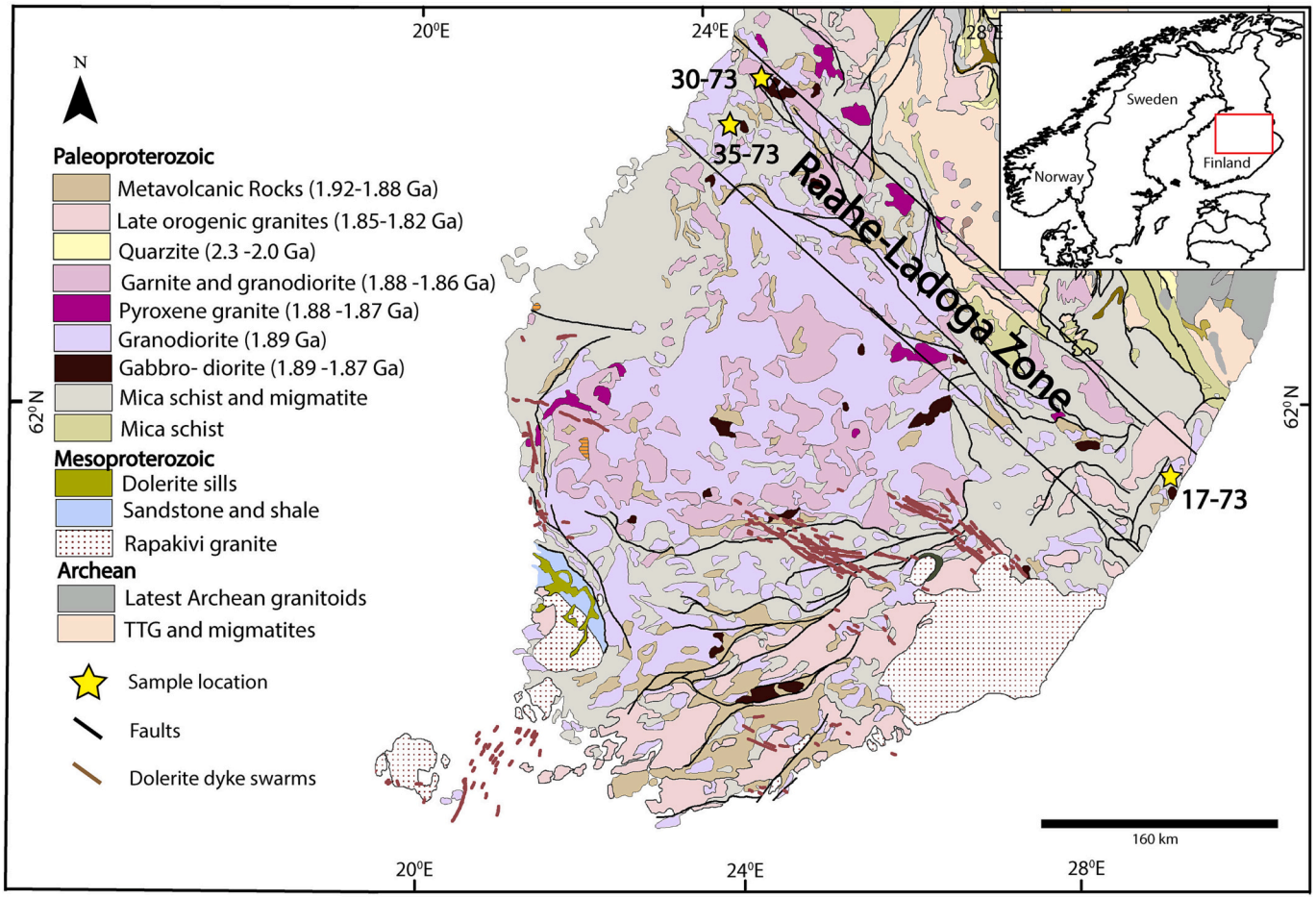

Fig. 3. Sample location map in the Raahe-Ladoga zone of Central Finland, after (Korsman, 1988; Kärki and Laajoki, 1995; Zaher et al., 2017). Star symbols show the location of the samples.

(Woodard et al., 2017). The Raahe-Ladoga zone separates reworked Archean cratons in the northeast of Finland from Palaeoproterozoic Svecofennian arc complexes to the southwest (Gaál and Gorbatschev, 1987; Korsman et al., 1999; Korsman, 1988; Woodard et al., 2017).

Two intrusions, described in Lethtovaara, (1976), were selected for this study: the Ylivieska gabbro and the Parikkala gabbro. The Ylivieska gabbro (samples 30–73 & 35–73) is located in the northwestern part of the Raahe-Ladoga zone (Vihanti-Pyhasakmi region). The gabbro outcrops over approximately 9 × 5 km and is surrounded by sandstone, felsic volcanic rocks and amphibolite (Salli, 1964). The intrusion is comprised of a layered gabbroic unit with a peridotite unit (1 km in diameter) in the SW part of the intrusion. The layered gabbroic unit is composed of norite, gabbronorite and olivine gabbronorite with hornblende gabbro and norite towards the margins (Makkonen et al., 2008). The peridotie unit is divided into an eastern and western unit; the eastern unit is composed of 10- to 100-m-thick peridotite, with a mineral assemblage of serpentinite and plagioclase-lherzolite and is separated by sheets of variably altered gabbros (Makkonen et al., 2008). Samples (30–73 and 35–73) were taken from the layered gabbroic unit of metamorphosed gabbro and gabbronorite.

The Parikkala gabbro (8 × 4 km; sample 17–73) is located in the southern part of the Raahe-Ladoga zone (Joroinen-Sulkava region) where it locally intrudes paragneisses. The intrusion is differentiated into three zones: hornblende-rich gabbros crop out in the northern part of the intrusion, gabbros in the centre have a high modal proportion of pyroxene, and olivine gabbros and olivine websterites dominate in the southern part of the intrusion (Mäkinen, 1987). Sample 17–73 is a coarse-grained, foliated hornblende gabbro. The main minerals are plagioclase and hornblende with chlorite, biotite, and minor carbonate as alteration minerals. This gabbro is inferred to have undergone regional metamorphism under amphibolite-facies conditions (Palosaari and Sokta, 1991). Häkli (1971) postulated that the intrusion underwent post-magmatic tilting to the north.

Both the Ylivieska and Parikkala grabbos were emplaced during the 1900–1880 Ma Svecofennian orogeny, which records both accretionary and collisional tectonic events (Gorbatschev and Bogdanova, 1993; Hermansson et al., 2008; Stephens and Andersson, 2015; Lahtinen, 1994; Lehtinen et al., 2005). The intrusions are *syn*-kinematic and were emplaced during the deformational and metamorphic peak (Mäkinen and Makkonen, 2004; Makkonen, 2005; Peltonen, 2005). The country rocks surrounding the intrusions were in most cases extensively metamorphosed and deformed during early Svecofennian orogenesis (Gaál and Gorbatschev, 1987; Kilpeläinen, 1998; Koistinen, 1981; Mäkinen and Makkonen, 2004). On a regional scale, granite gneiss and granodiorite yield U–Pb zircon ages of 1930 ± 15 Ma and 1880 ± 15 Ma in the Vihanti-Pyhäsalmi area of the northern part of the Raahe-Ladoga Zone (Helovuori, 1979). Post-tectonic gabbros from the Svecokarelian terrain in southern Finland are dated at ~1880 Ma (U–Pb on zircon; Patchett and Kouvo, 1986). The Ylivieska gabbro itself has yielded U–Pb zircon ages of 1883 ± 8 Ma (Patchett and Kouvo, 1986) and ~ 1920 Ma (Pesonen, 1972), while Vaasjoki and Sakko (1988) dated a gabbroic intrusive from the Vihanti area, which yielded a U–Pb age of 1901 ± 12 Ma. In the southern Raahe-Ladoga zone (Joroinen-Sulkava area), gabbros were emplaced between ~1910 and 1870 Ma as recorded by U–Pb zircon ages for mafic rocks (1880 ± 3 Ma from a norite, and 1912 ± 12 Ma and ~ 1869 Ma from a gabbro; Huhma,1986). The area underwent

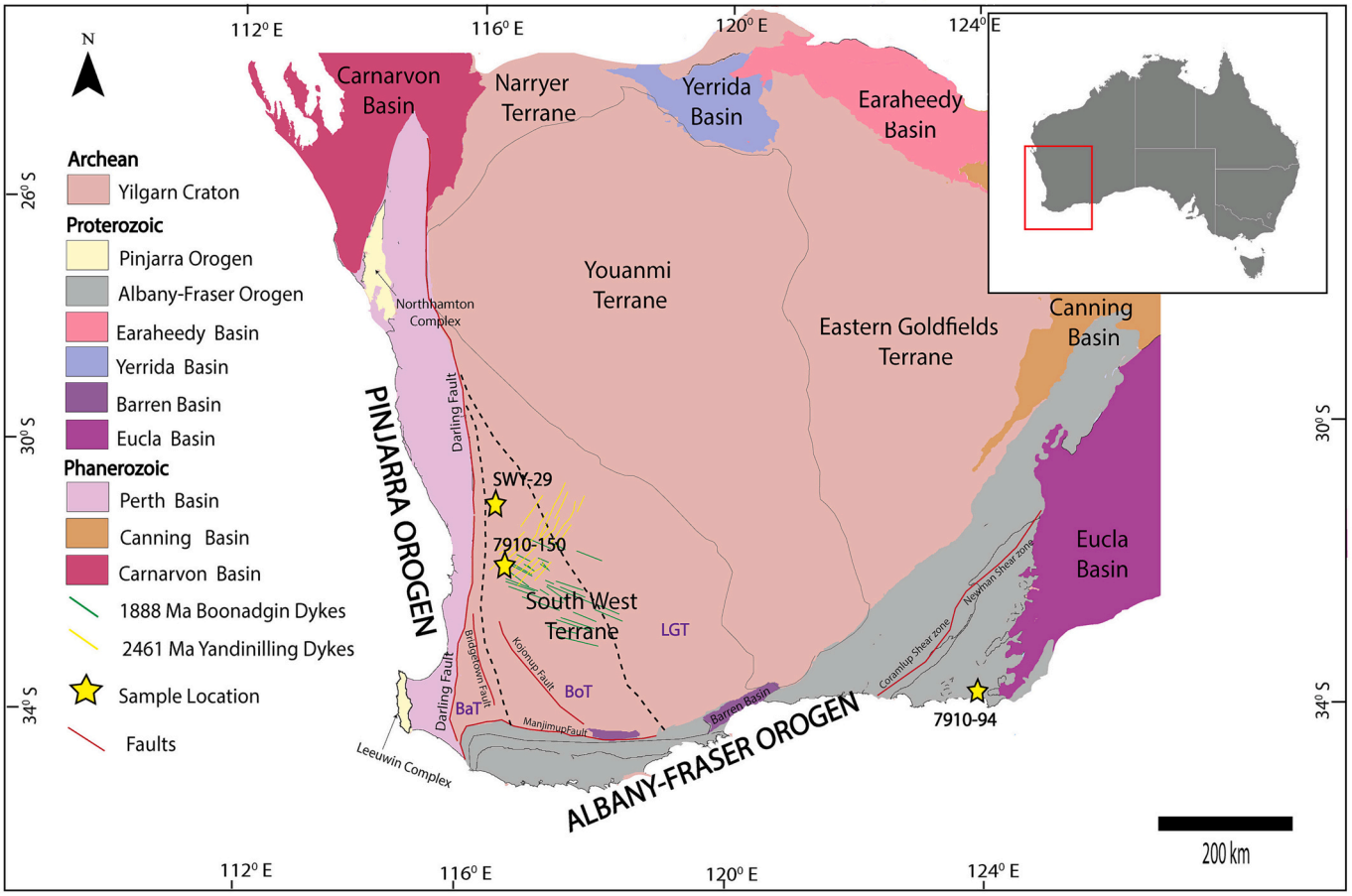

Fig. 4. Sample location map of the Nornalup zone, southeastern part of the Albany Fraser Orogeny (right) and location map of samples from the SW Yilgarn Craton (left). The maps are modified from Stark et al. (2018b), with sub-terrane boundaries indicated within the Southwest terrane after Wilde et al. (1996) and Lu et al. (2015): BaT = Balingup Terrane, BoT = Boddington Terrane, LGT = Lake Grace Terrane. Star symbols show the locations of the samples.

peak metamorphism and migmatization between ~1840 and 1810 Ma, as dated by zircon U–Pb (1810 ± 7 Ma and 1833 ± 22 Ma) and monazite U–Pb (~1820–1840 Ma) (Korsman et al., 1984; Vaasjoki and Sakko, 1988).

2.4. Yilgarn Craton and Albany Fraser Orogen, Western Australia

The Yilgarn Craton mostly comprises broadly linear, northwest-southeast trending Meso—Neoarchean granite-gneiss complexes and greenstone belts that are divided into a series of tectonostratigraphic terranes (Cassidy et al., 2006) (Fig. 4). These terranes include the Narryer, Southwest, and Youanmi terranes in the western part of the craton and the Eastern Goldfields Superterrane, which includes the Kalgoorlie, Kurnalpi, Burtville, and Yamarna terranes in the east of the craton (Cassidy et al., 2006). The Yilgarn Craton is bounded by the Paleo-Mesoproterozoic Albany Fraser Orogen (AFO) to the south and east, and the Darling Fault and Mesozoic Perth Basin to the west.

Two samples (metagabbro SWY-29 and dolerite dyke 7910–150) were taken from the Southwest Terrane (Fig. 4). This terrane has been exposed to higher grade metamorphism (low-pressure granulite facies conditions) compared to the terranes in the northeast of the Yilgarn Craton (Myers, 1993; Wilde et al., 1996). Based on regional geology and geophysical data, the Southwest Terrane is divided (from west to east) into the Balingup, Boddington and Lake Grace sub-terranes (Wilde et al., 1996). The higher metamorphic grade in the terrane is likely related to post-cratonization tilting of the crust, indicated by Rb—Sr biotite cooling ages that become younger towards the western margin of the Yilgarn Craton (Libby and De Laeter, 1998; Lu et al., 2015).

Metagabbro sample SWY-29, from the ore-hosting Gonneville intrusion at Julimar, within the Boddinton sub-terrane, is coarse-grained to pegmatitic and consists of subhedral plagioclase with pyroxene and other opaque and accessory minerals. A weighted mean $^{207}Pb/^{206}Pb$ zircon age of 2668 ± 4 Ma is interpreted as the igneous crystallization age of the metagabbro (GSWA 203747; Wingate et al., 2021).

Sample 7910–150 was taken from a dolerite dyke in the Boddinton sub-terrane, which is likely related to the N-E trending Yandinilling dyke swarm within the region (Stark et al., 2018b). The sample has an intergranular ophitic to sub-ophitic texture, comprising of plagioclase, pyroxene, opaque minerals (magnetite and ilmenite), quartz, and minor apatite. The dyke lacks any obvious tectonic foliation. Evidence for alteration includes the growth of brown amphibole along the grain boundaries of magmatic pyroxene or the complete replacement of pyroxene grains by a mixture of brown and green amphibole (Stark et al., 2018b). A baddeleyite U–Pb age of 2615 ± 6 Ma was obtained from a similar NE-trending mafic dyke in the Yandinilling dyke swarm in the SW Terrane (Stark et al., 2018b), which is inferred to have extended into the southwestern part of the craton.

Apatite grains were obtained from a gabbro (7710–94) located in the Nornalup Zone, in the southeastern part of the Albany Fraser Orogen (AFO) (Fig. 4). The AFO is a Paleo—Mesoproterozoic orogenic belt that developed along the southern and southeastern margins of the Yilgarn Craton, reworking the ancient cratonic core. The main lithologies of the AFO are amphibolite- to granulite-facies paragneiss and orthogneiss, intruded by late-tectonic plutons (Spaggiari et al., 2009; Myers, 1995). The Nornalup Zone is one of the litho-tectonic units of the AFO. Mesoproterozoic granitic intrusions from the Nornalup Zone fall into two discrete magmatic events, namely the ~1330–1280 Ma Recherche Supersuite (Myers, 1995), associated with collision Stage I of the AFO (Clark et al., 2000) and the ~1200–1125 Ma Esperance Supersuite, corresponding to intracratonic reactivation during Stage II of the AFO (Clark et al., 2000; Myers, 1993, 1995; Nelson et al., 1995; Clark et al., 1999). Gabbro sample 7710–94 is a co-genetic gabbroic enclave within a granite of the Esperance Supersuite. Seismic studies support phases of mingled granitic and mafic material that may have been intruded as a series of successive pulses (Spaggiari et al., 2014), while the geochemistry of the mafic components within the granite indicate minor contamination from the host granite and are compatible with a MORB-like source (Smithies et al., 2014).

3. Analytical methods

Apatite separates were mounted in 25 mm diameter epoxy disks. The samples were then ground with 1200, 2000 and 2500 grit sandpaper to expose the internal portions of grains and subsequently polished (up to 1 μm diamond finish). Apatite grains in each sample were dated by both the U–Pb and Lu—Hf systems across three analytical sessions. All analyses were conducted using a RESOlution 193 nm excimer laser-ablation system coupled to an Agilent 8900 ICP-MS/MS housed at Adelaide Microscopy, The University of Adelaide. A 'squid' mixing device (Laurin Technic) was used to smooth the pulses of aerosol between the laser and mass-spectrometer and N_2 gas (4 ml/min) was added to the carrier gas after the sample chamber but before the plasma in order to enhance signal sensitivity. In the first analytical session, trace element concentrations were acquired simultaneously with U–Pb isotopes using the analytical procedure outlined in Glorie et al. (2019) and Gillespie et al. (2018). The second analytical session used NH_3 (supplied as 10% NH_3 and 90% He) reaction gas to measure Lu—Hf isotopes, following the analytical approach outlined in Simpson et al. (2021). In the third analytical session, trace element data, U–Pb isotopes and Lu—Hf isotopes were all simultaneously acquired, with Lu—Hf analyses conducted on apatite grains that were large enough to accommodate a second ablation spot.

3.1. Apatite U–Pb geochronology

Apatite U–Pb and trace element analysis was conducted using a 30 μm spot size and 5 Hz repetition rate. In the first analytical session, MAD (ID-TIMS U–Pb age of 473.5 ± 0.7 Ma; Thomson et al., 2012; Chew et al., 2014) was used as a primary reference material to correct for instrumental drift and downhole fractionation. Mt. McClure apatite (ID-TIMS U–Pb age of 523.51 ± 1.47 Ma; Schoene and Bowring, 2006) was analysed as secondary standard to assess accuracy and our obtained weighted mean $^{206}Pb/^{238}U$ age of 526 ± 9 Ma, is in agreement with the recommended age (Supplement file 2). In the third analytical session, 401 apatite (ID-MC-ICP-MS U–Pb age of 530.3 ± 1.5 Ma; Thompson et al., 2016) was used as a primary reference material and OD306 apatite (LA-ICP-MS U–Pb age 1597 ± 7 Ma; Thompson et al., 2016) was used as a secondary standard. The calculated weighted mean $^{206}Pb/^{238}U$ age for OD306 apatite (1596 ± 7 Ma) from this session is within uncertainty of the recommended age.

Data reduction was performed using the LADR software(Norris and Danyushevsky, 2018). The U–Pb scheme within LADR was configured to remove initial Pb from the measured values of the reference material, achieved by subtracting the initial Pb from all the Pb isotope measurements using the Stacey and Kramers (1975) model. For the samples in this study, apatite U–Pb Terra-Wasserburg plots and U–Pb dates were calculated from the lower-intercept of unanchored (free regression) isochrons using IsoplotR (Vermeesch, 2018). Trace element abundances were simultaneously acquired and reduced in LADR using ^{43}Ca as internal standard and NIST 610 as the primary trace element reference material. The trace element data is presented on multi-element discrimination biplots, plotting Sr/Y ratios vs ∑LREE concentrations using the R script of O'Sullivan et al., (2020). The calculated ages for the reference materials are presented in Table 1 and associated concordia U–Pb plots for the standards are presented is Supplementary File 2.

3.2. Apatite Lu—Hf geochronology

Lu—Hf analyses were conducted on all apatite grains previously dated via U–Pb that were large enough to accommodate a second ablation spot and employed a beam size of 67 μm or 120 μm. The LA-ICP-MS/MS Lu—Hf dating approach uses NH_3 gas in the reaction-cell of the

Table 1
Secondary reference material ages from the three sessions.

Session	Mt. McClure apatite			OD-306 U-Pb			OD-306 Lu—Hf (uncorrected)			Bamble (corrected)			HR (corrected)		
	Age (Ma)	2σ (Ma)	MSWD (n)	Age (Ma)	2σ (Ma)	MSWD (n)	Age (Ma)	2σ (Ma)	MSWD (n)	Age (Ma)	2σ (Ma)	MSWD (n)	Age (Ma)	2σ (Ma)	MSWD (n)
1st Session	526	9	0.62(24)	–	–	–	–	–	–	–	–	–	–	–	–
2nd Session	–	–	–	–	–	–	1658	9	1.2 (31)	1097	7	0.68(32)	345	3	0.96(35)
3rd Session	–	–	–	1596	7	2.3(24)	1654	11	1.1 (23)	1097	9	0.9(22)	344	4	0.7 (23)
Expected*	523.51[1]	1.47	2.1	1597[2]	7	0.2	1597[2]	7	0.2	1097[3]	5	0.8 (70)	344[3]	2	0.7(96)

* The ratio between the measured and expected age for OD-306 is used as a session-dependant calibration factor the Lu—Hf ratios for each sample and secondary reference material.
[1] weighted-mean $^{207}Pb/^{235}U$ closure dates for apatite from Schoene and Bowring, 2006
[2] Isotope dilution apatite U–Pb age from Thompson et al., 2016
[3] Long-term reference apatite Lu—Hf ages from Glorie et al., 2022 (n) = number of analyses.

mass spectrometer. Reaction products of ^{176}Hf and ^{178}Hf are measured free from isobaric interferences at masses 258 and 260 amu, respectively. ^{177}Hf is subsequently calculated from ^{178}Hf, assuming natural abundances. ^{176}Lu is calculated from the measured ^{175}Lu signal using the natural (invariant) isotope ratio (details in Simpson et al., 2021).

The Lu and Hf isotopic data were reduced in LADR (Norris and Danyushevsky, 2018). For both Lu—Hf analytical sessions, NIST 610 (Nebel et al., 2009) was used as the primary standard, and OD306 apatite (1597 ± 7 Ma; Thompson et al., 2016) was used to correct for matrix-induced fractionation (Glorie et al., 2022; Glorie et al., 2023). In-house apatite reference materials Bamble (Lu—Hf age: 1097 ± 5 Ma) and Harts Range (Lu—Hf age: 343 ± 2 Ma) were analysed to assess accuracy (Glorie et al., 2023). Lu—Hf ages were calculated from inverse isochrons using IsoplotR (Vermeesch, 2018; Li and Vermeesch, 2021),

Table 2
Summary of all U–Pb and Lu—Hf ages. (1) U–Pb zircon/baddeleyite age from Krogh et al. (1984); (2) U–Pb zircon age from Corfu Corfu and Lightfoot, (1996); (3) U–Pb zircon age from Leterrier et al. (1994); (4) U–Pb zircon ages from Archanjo et al. (2013); (5) U–Pb monazite ages from Souza de et al. (2006); (6) U–Pb zircon ages from McReath et al. (2002); (7) U–Pb zircon ages from Sá et al. (2013); (8) U–Pb zircon ages from Nascimento Souza and Oliveira, (2022); (9) Rb—Sr age from Galindo (1993); (10) U–Pb zircon ages from Vaasjoki and Sakko, (1988); (11) U–Pb zircon ages from Huhma (1986); (12) U–Pb zircon age from Helovuori (1979); (13) U–Pb zircon age from Patchett and Kouvo (1986); (14) U–Pb Zircon ages from GSWA 184374 Kirkland et al. (2012); (15) $^{207}Pb/^{206}Pb$ zircon age from GSWA 203747 Wingate et al. (2021); (16) U–Pb Baddeleyite ages from Stark et al. (2018a); (17) U–Pb Baddeleyite ages from Stark et al. (2018b). (n) = number of analyses.

Sample	Latitude/Longitude	Analytical session U-Pb	Reference age Age (Ma)	Reference age 2σ (Ma)	Ap U-Pb Iso Age (Ma)	Ap U-Pb 2σ (Ma)	Ap U-Pb MSWD (n)	Analytical session Lu-Hf	Ap Lu-Hf Iso Age (Ma)	Ap Lu-Hf 2σ (Ma)	Ap Lu-Hf MSWD (n)
Superior Craton, Canada											
OOML11	46°32′37”N / 81°27′2”W	3rd Session	1850(1)	3	1919	76	2(37)	3rd Session	1850	44	1.7(40)
OOML13	46°32′37”N / 81°27′2”W	3rd Session	1849(2)	2	1833	45	1.2(30)	3rd Session	1879	22	1.3(41)
OOML19	46°32′37”N/ 81°27′2”W	3rd Session			1877	54	2.5 (39)	3rd Session	1874	22	1.4(43)
Borborema Province, NE Brazil											
CR-137	06°47′12”S / 37°23′35”W	3rd Session	579(3)	7	568	8	3.2(30)	3rd Session	605	25	1.5(35)
			599(4)	16							
			595(4)	3							
			553(5)	10							
CR-138	05°47′35”S / 37°42′35”W	3rd Session	593(6)	5	553	14	1.6(21)	3rd Session	615	23	1.4(21)
			601(7)	11							
			587(8)	2							
			564(8)	4							
			545(9)	7							
CR-146	06°13′47”S / 36°34′12.8”W	1st Session	579(3)	7	551	9	3.1 (33)	2nd Session	600	11	1.4(20)
			599(4)	16							
			595(4)	3							
			553(5)	10							
Fennoscandian Shield, Finland											
17–73	61°33′55”N / 29°45′26″E	3rd Session	1901(10)	12	1667	30	2(34)	3rd Session	1824	83	0.83(17)
			1880(11)	3							
			1912(11)	12							
30–73	64°15′36”N / 24°49′16″E	1st Session	1930(12)	15	1714	34	1.9(27)	2nd Session	1907	39	1.3(26)
35–73	64°2′30”N / 24°31′12″E	3rd Session	1880(12)	15	1782	8	0.72(40)	3rd Session	1899	35	0.83(35)
			1883(13)	8							
Albany Fraser Orogen, Western Australia											
7710–94	33°53′30”S / 122°53′30″E	1st Session	1198(14)	11	1133	11	1.1(33)	2nd Session	1159	12	1.4(42)
SouthWest Yilgarn Craton, Western Australia											
SWY-29	31°24′13”S / 116°19′168″E	1st Session	2668(15)	4	661	17	3(21)	2nd Session	1134	27	2.1(33)
7910–150	32°16′46”S / 116°17′19″E	1st Session	1390(16)	3	567	12	4.6(95)	2nd Session	2677	128	0.65(5)
			2615(17)	6					991	66	2.2(22)

anchored to an initial $^{177}Hf/^{176}Hf$ ratio of 3.5 ± 0.05, which captures the maximum variability of the terrestrial Hf isotopic reservoir (Simpson et al., 2021; Glorie et al., 2022, 2023; Vervoort, 2014; Fisher and Vervoort, 2018). The reported 95% confidence uncertainties for the Lu—Hf ages are fully propagated, including the uncertainty on the measured age for the correction standard OD306. The calculated ages for the reference materials are presented in Table 1 and associated isochron and weighted mean age calculations are presented is Supplementary File 2.

4. Results

The apatite U–Pb and Lu—Hf results for the four different areas are described below and are summarized in Table 2. The complete datasets can be found in Supplementary File 3 (U-Pb + trace elements) and Supplementary File 4 (Lu—Hf).

4.1. Sudbury Igneous Complex (SIC)

The Sr/Y versus LREE biplot categorizes all analysed apatites fom the SIC in the mafic field of the diagram, suggesting their trace element compositions preserve a primary signal from their mafic host lithologies and have not been modified by post-crystallization processes (Fig. 5a).

The apatite U–Pb and Lu—Hf ages from the three samples from the SIC are presented in Fig. 6. For sample 00ML11, a total of 37 out of 38 U–Pb apatite analyses plot along a linear array on Tera-Wasserburg concordia with a $^{238}U—^{206}Pb$ lower intercept age of 1919 ± 76 Ma (MSWD = 2). Sample 00ML13, yields a similar variability in $^{207}Pb/^{206}Pb$ ratios, defining a lower intercept age of 1833 ± 45 Ma (n = 30, MSWD =1.2). Sample 00ML19 has slightly more radiognic $^{207}Pb/^{206}Pb$ ratios, yielding a U–Pb lower intercept age of 1877 ± 54 Ma (n = 39, MSWD = 2.5). Hence, taking the ~2.5–4% uncertainties into account, all U–Pb

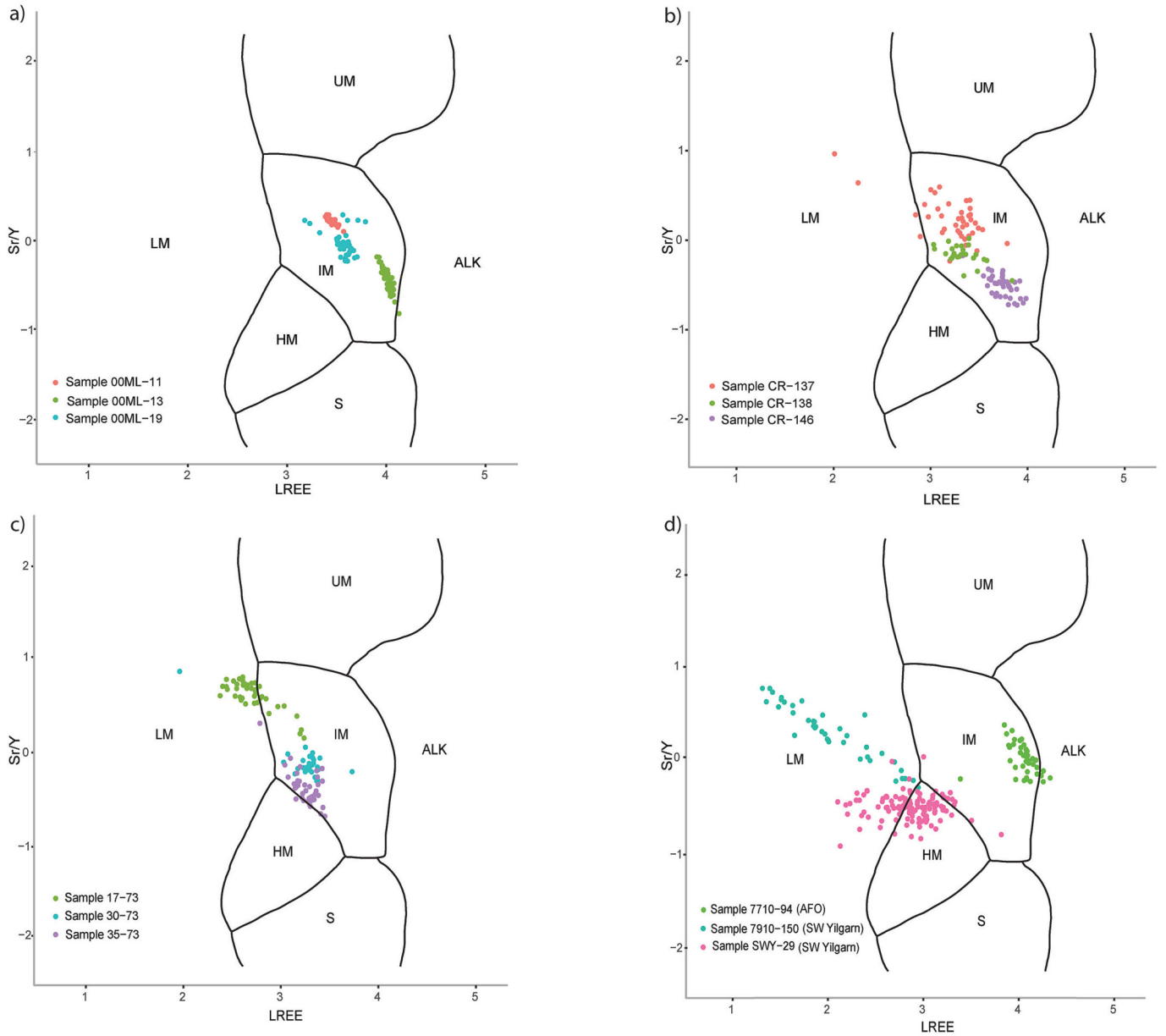

Fig. 5. Multi-element discrimination biplot (Sr/Y vs LREE) from O'Sullivan et al. (2020) for the analysed apatites. (a) samples from Sudbury Igneous Complex; (b) samples from Piranhas- Seridó Domain (PSD), Borborema Province, NE Brazil; (c) samples from the Raahe-Ladoga zone in Central Finland; and (d) samples from the Albany Fraser Orogen and SW Yilgarn Craton. Abbreviations for each lithological discrimination field are: ALK = alkali-rich igneous rocks; IM = mafic I-type granitoids and mafic igneous rocks; LM = low-and medium-grade metamorphic and metasomatic; HM = partial-melts/ leucosomes/high-grade metamorphic; S = S-type granitoids and high aluminium saturation index (ASI) "felsic" I-types; UM = ultramafic rocks including carbonatites, lherzolites and pyroxenites.

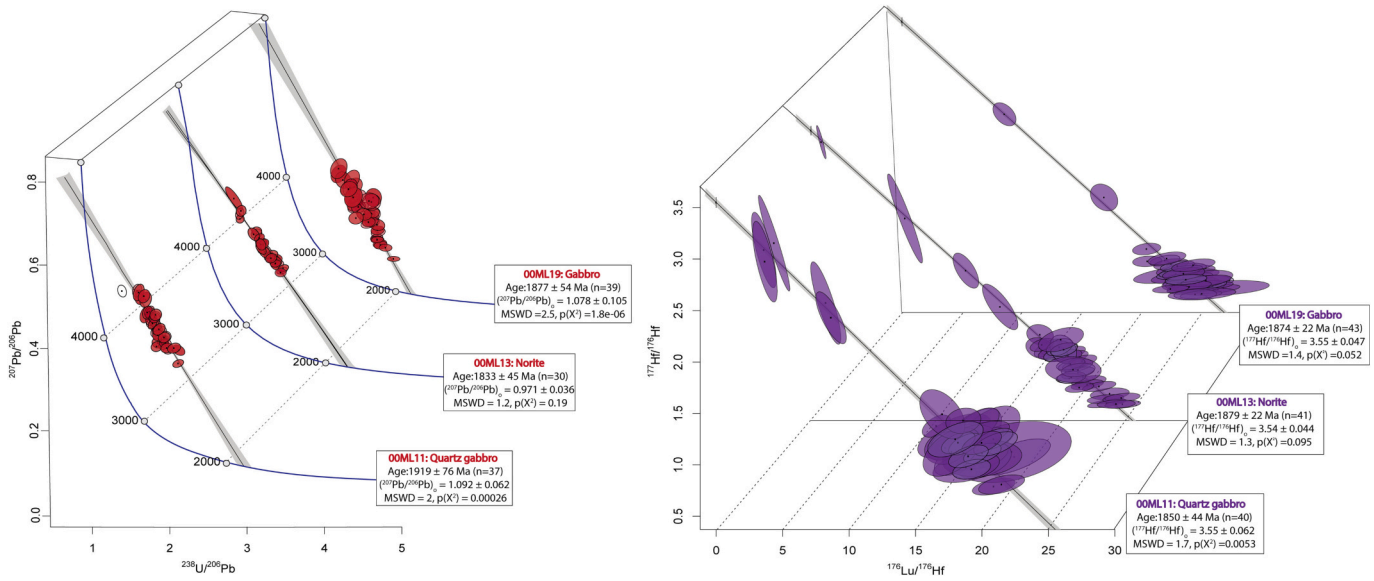

Fig. 6. Stacked apatite U–Pb Tera-Wasserburg plots (left, in red) and stacked Lu—Hf isochron plots (right, in purple) for samples from the Sudbury Igneous Complex (calculated in IsoplotR; Vermeesch, 2018). MSWD = mean squared weighted deviation and P(χ^2) = Chi-squared probability for a single data population. (For interpretation of the references to colour in this figure legend, the reader is referred to the web version of this article.)

dates overlap within uncertainty.

Apatite in sample 00ML11 has Lu concentrations of 2.3–3.9 ppm and $^{177}Hf/^{176}Hf$ ratios ranging between 0.7 and 1.5, with 12.5% of the analyses having slightly higher values between 2.5 and 3.2. The Lu—Hf isotopic ratios define a Lu—Hf isochron age of 1850 ± 44 Ma (n = 40, MSWD = 1.7). For sample 00ML13, the Lu concentrations vary from 4 to 5.5 ppm and $^{177}Hf/^{176}Hf$ ratios range between 0.4 and 3.4 with most ratios ≤1.5. The resulting Lu—Hf isochron age is 1879 ± 22 Ma (n = 41, MSWD = 1.3). For sample 00ML19, the Lu—Hf data define a Lu—Hf isochron age of 1874 ± 22 Ma (n = 43, MSWD = 1.4) with Lu concentrations varying from 1.5 to 4.7 ppm and $^{177}Hf/^{176}Hf$ ratios mostly between 0.4 and 1.5 with ~5% analyses between 1.5 and 2.4. Hence, the Lu—Hf ages are in good agreement with the U–Pb ages but are more consistent and with smaller uncertainties (~1–2%).

4.2. Borborema Province

Similar to the Sudbury Igneous Complex, the Sr/Y versus LREE biplot confirms that all but two apatite grains from the Borborema Province preserve primary mafic trace element compositions (Fig. 5b).

The U–Pb and Lu—Hf ages for all samples from the Borborema Province are presented in Fig. 7. Apatites from leucogabbro sample CR-137 yield a lower intercept age of 568 ± 8 Ma (n = 28, MSWD = 3.2). Leuconorite samples CR-138 and CR-146 yield a U–Pb lower intercept age of 553 ± 14 Ma (n = 21, MSWD = 1.6) and 551 ± 9 Ma (n = 33, MSWD = 3.1), respectively. In summary, apatite in all three samples produce consistent latest Ediacaran U–Pb ages.

The Lu—Hf results, however, produce significantly different apatite ages. All samples have relatively radiogenic $^{177}Hf/^{176}Hf$ ratios, ranging from 0.1 to 1.2. Sample CR-137 yields a Lu—Hf isochron age of 605 ±

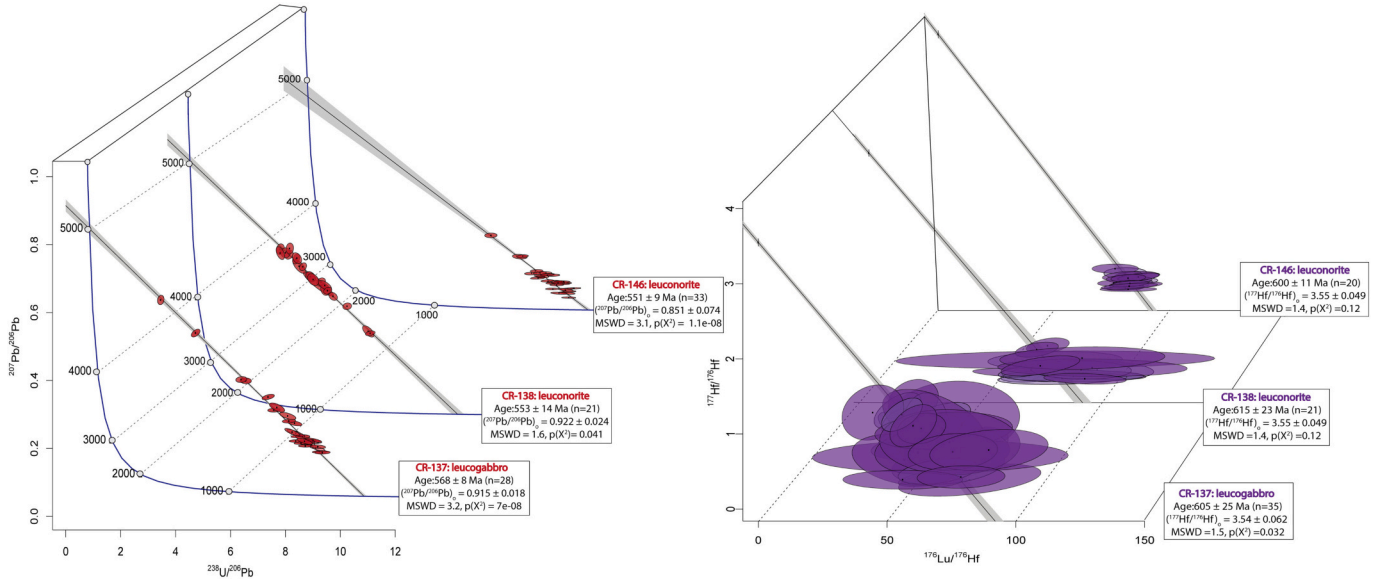

Fig. 7. Stacked apatite U–Pb Tera-Wasserburg plots (left, in red) and stacked Lu—Hf isochron plots (right, in purple) for samples from the Piranhas- Seridó Domain (PSD), Borborema Province, NE Brazil (calculated in IsoplotR; Vermeesch, 2018). MSWD = mean squared weighted deviation and P(χ^2) = Chi-squared probability for a single data population. (For interpretation of the references to colour in this figure legend, the reader is referred to the web version of this article.)

25 Ma (n = 35, MSWD = 1.5) with Lu concentraions between 1.1 and 7 ppm and $^{177}Hf/^{176}Hf$ ratios between 0.3 and 1.4. For sample CR-138, a total of 15 out of 21 analyses yield strongly radiogenic $^{177}Hf/^{176}Hf$ ratios <0.3 (Lu ~ 4.6–14 ppm) and produce an isochron Lu—Hf age of 615 ± 23 Ma (MSWD = 1.4). Sample CR-146 (13/20 analyses with $^{177}Hf/^{176}Hf$ ratios between 0.1 and 0.8 and Lu ~ 7.9–17.3 ppm) yields an isochron Lu—Hf age of 600 ± 11 Ma (n = 20, MSWD = 1.4). Hence, apatite from these samples yield consistent early Ediacaran apatite Lu—Hf ages, which do not overlap within uncertainty with their equivalent U–Pb dates.

4.3. Fennoscandian Shield, Finland

The Sr/Y versus LREE biplot for the Ylivieska gabbro reveals that all but one of the analysed apatite grains are categorized as mafic based on their trace element compositions. For the Parikaala Gabbro, the apatite trace element compositions define a mixing line between the mafic and low-grade metamorphic fields in the discrimination biplot, suggesting a secondary event may have disturbed the apatite trace element compositions (Fig. 5c).

The U–Pb and Lu—Hf ages for all samples from the Fennoscandian Shield are presented in Fig. 8. Apatites from the Ylivieska gabbro (30–73 & 35–73) yield U–Pb lower intercept ages of 1714 ± 34 Ma (n = 27, MSWD = 1.9) and 1782 ± 8 Ma (n = 40, MSWD = 0.72), respectively. For the Parikkala Gabbro (17–73), the U–Pb lower intercept age of 1667 ± 30 Ma (n = 34, MSWD = 2) is significantly younger than the lower intercept age obtained from the Ylivieska gabbro.

The $^{177}Hf/^{176}Hf$ ratios for the Ylivieska gabbro are highly variable (~0.5–2) and the Lu—Hf isotopic data yield consistent isochron ages of 1907 ± 39 Ma (30–73; n = 26, MSWD = 1.3) and 1899 ± 35 Ma (35–73, n = 35, MSWD = 0.83), with Lu concentrations between 2.3 and 6.9 ppm. The Lu—Hf data for the Parikkala Gabbro are much more radiogenic ($^{177}Hf/^{176}Hf$ ratios <0.5), defining an inprecise isochron age of 1824 ± 83 Ma (n = 17, MWSD = 0.83) with Lu concentrations between 0.7 and 2.6. The large uncertainty reflects the generally low Lu concentration of apatite in this sample. The Lu—Hf apatite ages from the Ylivieska intrusion are considerably older than their respective U–Pb dates. The Lu—Hf age for the Parikkala Gabbro is older than its U–Pb age, but consistent within uncertainty with the oldest U–Pb age of the Ylivieska Gabbro.

4.4. SW Yilgarn Craton and Albany Fraser Orogen, Western Australia

The Sr/Y versus LREE biplot for gabbro sample 7710–94 (Sr/Y ratio = 1.13 & LREE = 11,733) from the Albany Fraser Orgen classifies all apatite grains as mafic. In contrast, apatite from the two samples from the southwest Yilgarn Craton (South West Terrane) are classified as low-grade metamorphic (dolerite 7910–150, Sr/Y ratio = 2.50 & LREE = 199) and high-grade metamorphic (metagabbro SWY29, Sr/Y ratio = 0.33 & LREE = 928), and thus do not preserve the primary trace element compositions of their mafic protoliths (Fig. 5d).

The U–Pb and Lu—Hf ages for all three samples from Western Australia are presented in Fig. 9. Sample 7710–94 from the Albany Fraser Orogen produced a U–Pb lower intercept age of 1133 ± 11 Ma (n = 33, MSWD = 1.1). The U–Pb lower intercept ages for samples SWY-29 and 7910–150, both from the SW Yilgarn Craton, are more dispersed with high MSWD values. Filtering the apatite data for sample SWY-29 with a criterion of log(LREE) ppm < 2.65 (which effectively selects only low-grade metamorphic apatite), a U–Pb lower intercept age of 661 ± 17 Ma (n = 21, MSWD = 3) is obtained. Sample 7910–150 yields a U–Pb lower intercept age of 567 ± 12 Ma (n = 95, MSWD = 4.6).

Sample 7710–94 from the Albany Fraser Orogen yields $^{177}Hf/^{176}Hf$ ratios between 0.1 and 0.9 and Lu concentrations between 3.6 and 16 ppm. The Lu—Hf isotopic ratios define a Lu—Hf isochron age of 1159 ± 12 Ma (n = 42, MSWD = 1.4). The Lu—Hf data for sample SWY-29 (SW Yilgarn Craton) define a Lu—Hf isochron age of 1134 ± 27 Ma (n = 33, MSWD = 2.1) with Lu concentraions ranging between 3.3 and 8.1 ppm with highly variable $^{177}Hf/^{176}Hf$ ratios between 0.2 and 3.8.

Sample 7910–150 (SW Yilgarn Craton) yields $^{177}Hf/^{176}Hf$ ratios between 0.3 and 3.9 with Lu concentrations of 0.5–9.9 ppm. Four out of 27 apatites analysed for Lu—Hf isotopes yield Archean ages, constrained by an isochron age of 2677 ± 128 Ma (n = 5, MSWD = 0.65). The remaining analyses define a more scattered Lu—Hf isochron with a lower intercept age of 991 ± 66 Ma (n = 22, MSWD = 2.2).

5. Discussion

Based on the four cases studies, we evaluate the apatite Lu—Hf systematics compared to the apatite U–Pb systematics in the analysed (meta-)mafic rocks. A summary time-space plot of all the data obtained in this study and previously published literature dates is presented in

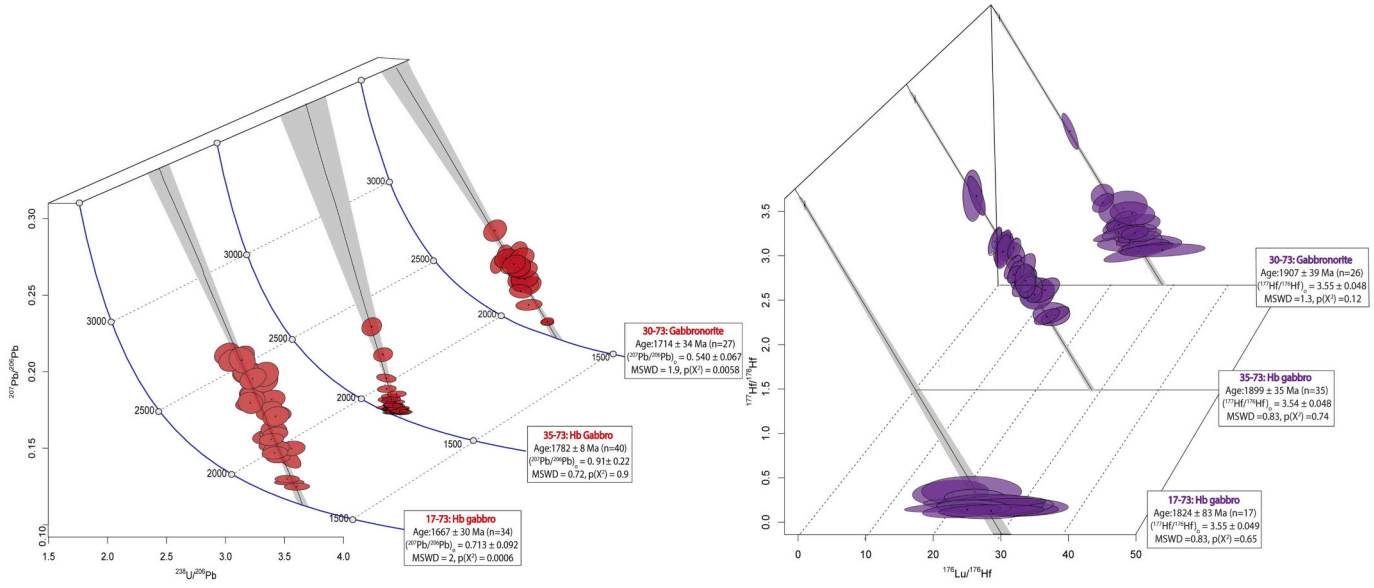

Fig. 8. Stacked apatite U–Pb Tera-Wasserburg plots (left, in red) and stacked Lu—Hf isochron plots (right, in purple) for samples from the Raahe-Ladoga zone in Central Finland (calculated in IsoplotR; Vermeesch, 2018). MSWD = mean squared weighted deviation and P(χ^2) = Chi-squared probability for a single data population. (For interpretation of the references to colour in this figure legend, the reader is referred to the web version of this article.)

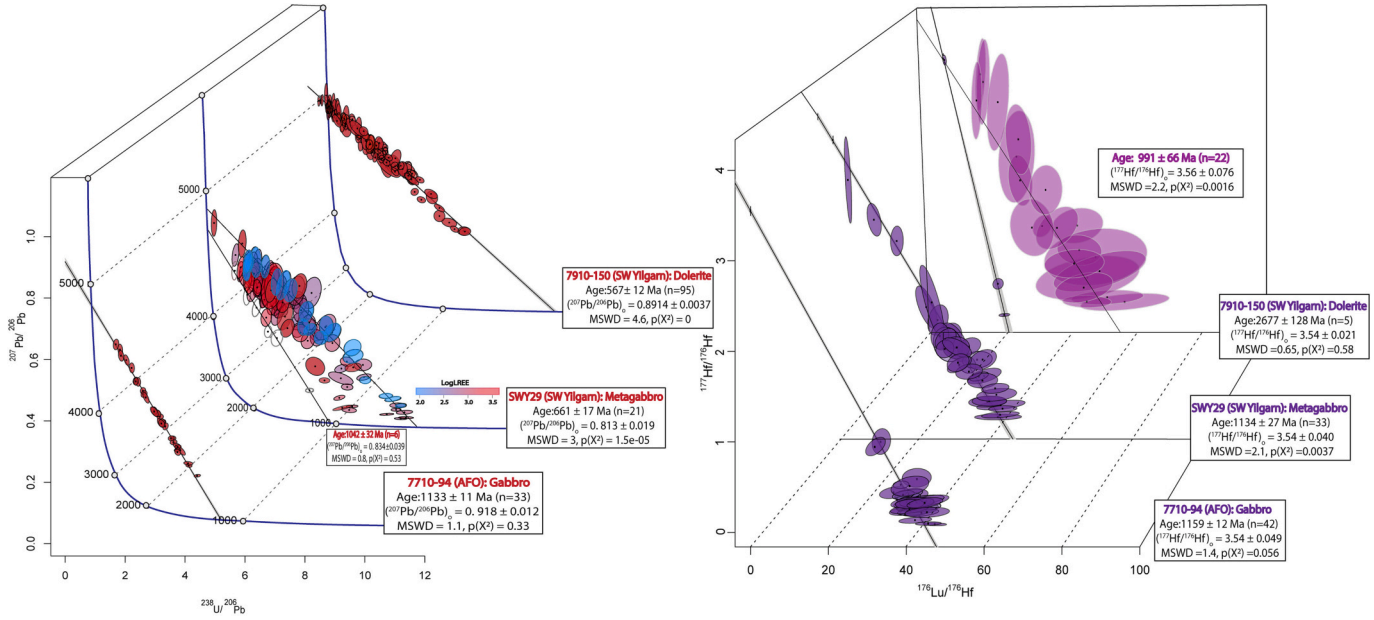

Fig. 9. Stacked apatite U–Pb Tera-Wasserburg plots (left, in red) and stacked Lu—Hf isochron plots (right, in purple) for samples from the Albany Fraser Orogen and SW Yilgarn Craton (calculated in IsoplotR; Vermeesch, 2018). MSWD = mean squared weighted deviation and P(χ^2) = Chi-squared probability for a single data population. For the U–Pb plots in sample SWY-29, the data is colour-coded according to the apatite LREE composition. Only grains with log(LREE) ppm < 2.65 (which effectively selects only low-grade metamorphic apatite) were plotted for the youngest lower intercept age. The oldest lower intercept age is denoted by non-filled ellipses. (For interpretation of the references to colour in this figure legend, the reader is referred to the web version of this article.)

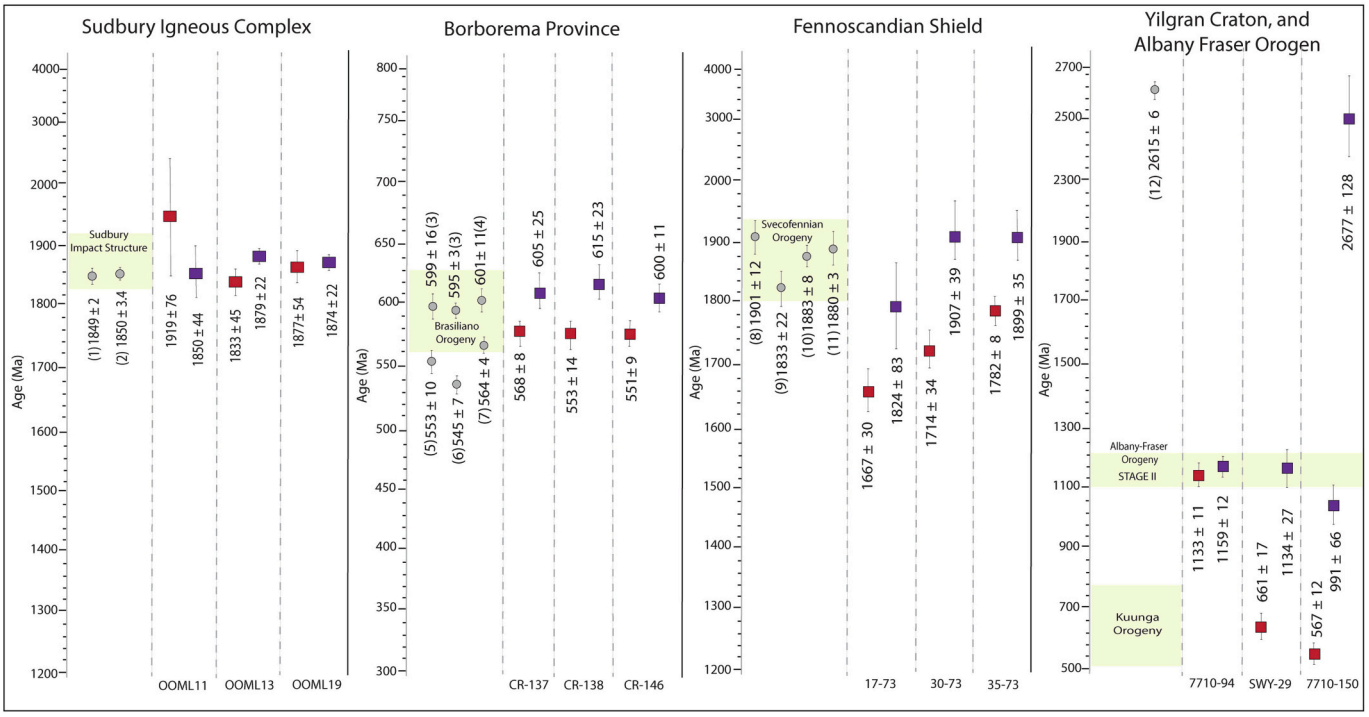

Fig. 10. Time-space plot of the ages obtained from this study: U–Pb apatite ages (red) and Lu—Hf ages (purple) are illustrated by square symbols. All reference ages are presented by circle symbols in grey: (1) U–Pb baddeleyite qz-diorite Corfu and Lightfoot, 1996; (2) U–Pb Zircon ages from mafic norite Krogh et al. 1984; (3) U–Pb zircon ages from Archanjo et al. (2013); (4); U–Pb zircon ages from Sá et al. (2013); (5) U–Pb monazite ages from Souza de et al. (2006); (6) Rb—Sr age of 545 ± 7 Ma from Galindo (1993); (7) U–Pb zircon ages Nascimento Souza and Oliveira, 2022; (8) U–Pb zircon ages from Vaasjoki and Sakko (1988); (9) U–Pb zircon age from Korsman et al. (1984); (10) U–Pb zircon age from Patchett and Kouvo (1986); (11) U–Pb zircon ages from Huhma (1986); (12) U–Pb baddeleyite ages from Stark et al. (2018b). (For interpretation of the references to colour in this figure legend, the reader is referred to the web version of this article.)

Fig. 10.

5.1. Sudbury Igneous Complex (Canada): Lu—Hf and U–Pb systematics of mafic apatite in an area with a simple thermal history

Apatite from the Sudbury Igneous Complex preserves primary mafic trace element compositions (Fig. 5a). The Sudbury Igneous Complex is considered to have formed during a meteorite impact at ~1850 Ma (Krogh et al., 1984). Zircon and baddeleyite grains have produced precise concordant U–Pb ages of 1850 ± 3 Ma and 1849 ± 1 Ma (Krogh et al., 1984). The new apatite U–Pb ages of 1919 ± 76 Ma, 1833 ± 45 Ma and 1877 ± 54 Ma and the more precise apatite Lu—Hf isochron ages of 1850 ± 44 Ma, 1879 ± 22 Ma, and 1874 ± 22 Ma (Fig. 6.) are in good agreement with the expected crystallization age. This implies the U–Pb and Lu—Hf apatite isotopic systems have not been disturbed by subsequent thermal events (such as those related to the Grenville Orogeny). This case study demonstrates the ability of the Lu—Hf system in apatite to provide robust primary crystallization ages for mafic igneous rocks.

5.2. Borborema Province (Brazil): decoupling between the Lu—Hf and U–Pb systems

Samples from mafic intrusions in the Piranhas-Serido Domain (PSD) of the Borborema province yield apatite U–Pb ages that are younger than their corresponding Lu—Hf ages. Samples CR-137 and CR-146 from the shoshonitic suite yield U–Pb ages of 568 ± 8 Ma and 551 ± 9 Ma and Lu—Hf ages of 605 ± 25 Ma and 600 ± 11 Ma, respectively. The Lu—Hf ages are in agreement with the zircon U–Pb ages of 599 ± 16 Ma and 595 ± 3 Ma from nearby gabbronorite samples from the same magmatic suite (Archanjo et al., 2013). The apatite U–Pb ages are similar to the published zircon U–Pb age of a nearby diorite dike (579 ± 7 Ma; Leterrier et al., 1994) and slightly older than a monazite U–Pb age (553 ± 10 Ma; Souza de et al., 2006), suggesting that the U–Pb system might have been (partially reset) by subsequent thermal events. Similarly, sample CR-138, taken from the alkaline charnockitic Umarizal pluton, yields an apatite U–Pb age of 553 ± 14 Ma and a Lu—Hf age of 615 ± 23 Ma. The Lu—Hf age is in agreement with previously published zircon ages for this intrusion (593 ± 5 Ma, 601 ± 11 Ma; 587 ± 2 Ma; McReath et al., 2002; Sá et al., 2013; Nascimento Souza and Oliveira, 2022) and predates the timing of high-temperature metamorphism and migmatization in the contact aureole (581 ± 4 Ma). The apatite U–Pb age is significantly younger and in good agreement with a Rb—Sr age (545 ± 7; Galindo, 1993) for the same intrusion.

Hence, the Lu—Hf system remained undisturbed in apatite from the sampled mafic rocks and accurately dates the timing of Ediacaran magmatic emplacement. In contrast, the U–Pb system in apatite in the same samples has been reset and yields ages similar to regional Rb—Sr ages, which together likely reflect cooling ages following pluton emplacement and high-grade metamorphism. The apatite grains from this case study preserve primary mafic trace element compositions (Fig. 5b), indicating that they did not recrystallize but lost Pb by volume diffusion during the post-magmatic thermal history. Hence, the diffusion of Pb in these apatite grains is decoupled from diffusion of REEs, consistent with theoretical calculations and empirical observations that Pb diffuses at lower temperatures than REEs in apatite (Cherniak, 2000; Glorie et al., 2023). Consequently, when apatite preserves a primary mafic REE composition, the Lu—Hf system can accurately date magmatic crystallization whereas the U–Pb system might record post-magmatic isotopic disturbances.

5.3. Fennoscandian Shield (Finland): Apatite Lu—Hf and U–Pb systematics in a strongly deformed terrane

Apatite from gabbros in the Fennoscandian study area have contrasting trace element compositions, reflecting different degrees of post-magmatic modification by metamorphism and deformation. Samples taken from the largely undeformed Ylivieska gabbro (30–73 and 35–73), in the northwestern part of the Raahe-Ladoga zone, record primary mafic apatite trace element compositions (Fig. 5c) and yield U–Pb ages of 1714 ± 34 Ma and 1782 ± 8 Ma and Lu—Hf ages of 1907 ± 39 Ma and 1899 ± 35 Ma. Concordant zircon ages of ~1920 Ma (Pesonen, 1972) and 1883 ± 8 Ma (Patchett and Kouvo, 1986) obtained for the Ylivieska gabbro, suggests that the Lu—Hf ages correspond with the early Svecofennian zircon crystallization ages (Gorbatschev and Bogdanova, 1993; Hermansson et al., 2008; Stephens and Andersson, 2015). The obtained apatite U–Pb ages are younger, suggesting that post-magmatic metamorphism induced a thermal reset of the U–Pb system in apatite while the Lu—Hf system remained undisturbed.

Furthermore, apatite from the foliated Parikkala gabbro from Joroinen-Sulkava have depleted LREE and Y compositions compared to apatite from the Ylivieska gabbro. Consequently, apatite trace element compositions plot along a mixing line between the primary mafic igneous and low-grade metamorphic fields, consistent with (partial) recrystallization. The obtained apatite U–Pb age of 1667 ± 30 Ma and the Lu—Hf age of 1824 ± 83 Ma are both younger than the published U–Pb zircon crystallization age (1880 ± 3 Ma; Huhma, 1986), although the Lu—Hf age overlaps with the zircon U–Pb age when considering its large uncertainty.

Vaasjoki and Sakko (1988) suggested that the Svecofennian orogen was caused by the collision of Paleoproterozoic oceanic and Archaean continental plates between ~1930 and ~ 1850 Ma. Following a period of tectonic quiescence, magmatic underplating induced migmatization at ~1830–1810 Ma in present-day southern Finland, followed by emplacement of ~1800–1780 Ma post-tectonic granitoids in the Gothian area of Sweden from ~1750 Ma onwards. The apatite Lu—Hf age obtained for the Parikkala gabbro is very similar to zircon and monazite U–Pb ages dating migmatization in the area at ~1840 Ma and 1810 Ma (Korsman et al., 1984; Vaasjoki and Sakko, 1988), but is also within uncertainty of the zircon U–Pb crystallization age. Hence, the obtained Lu—Hf age likely reflects a composite age comprising a mixture of primary igneous and recrystallized metamorphic apatite. The apatite U–Pb ages in the Fennoscandian study area are interpreted to record thermal resetting after peak metamorphism and can thus be interpreted as cooling ages.

5.4. SW Terrane, Yilgarn Craton: isotopic resetting in a complex, hot terrane

Mafic sample 7710–94 from the Nornalup zone in the south-eastern part of the Albany Fraser Orogen yielded an apatite U–Pb age of 1133 ± 11 Ma and a Lu—Hf age of 1159 ± 12 Ma. Stage II of the Albany Fraser Orogen, involved widespread high grade metamorphsim and granite emplacment between ~1300 Ma and ~1100 Ma and is considered a major tectonothermal event (Nelson et al., 1995; Black et al., 1992; Pidgeon, 1990). The synchronous emplacement of the granites and gabbros of Esperance Supersuite coincided with Stage II in the AFO. The apatite Lu—Hf and U–Pb dates for the sampled gabbro enclave are internally consistent and also agree with published zircon U–Pb crystallization ages for the Esperance Supersuite of 1135 ± 56 Ma (GSWA 833667, Nelson et al., 1995) and 1198 ± 11 Ma (GSWA 184374, Kirkland et al., 2012; Myers, 1995; Nelson et al., 1995; Clark et al., 2000). The new apatite dates for this sample serve as a reference for understanding the systematics of the more complex Lu—Hf and U–Pb systematics in apatite from the adjacent Yilgarn Craton.

For meta-gabbro sample SWY-29, a Lu—Hf isochron age of 1134 ± 27 Ma ($n = 33$, MSWD = 2.1) was obtained. Given the sample was taken from an Archean gabbro (2668 ± 4 Ma; Wingate et al., 2021), the Lu—Hf apatite system must have been reset. The apatite trace element data is consistent with apatite (re)growth during high-temperature metamorphism (Fig. 5d), and concequently, the apatite Lu—Hf age is interpreted to date this metamophic overprint. The reset apatite Lu—Hf

age may be a result of recrystallization and/or thermal diffusion, given that Stage II of the AFO is associated with widespread UHT conditons. Given the Lu—Hf closure temperature in apatite (~660–730 °C; Gloire et al., 2023), we suggest that this metamorphic event exceeded 730 °C to allow for complete isotopic reequilibration. The reset Lu—Hf age corresponds to the timing of Stage II of the Albany-Fraser Orogeny, which reworked the SW Yilgarn Craton margin (Clark et al., 2000; Liebmann et al., 2023).

Sample 7910–150 was taken from a dolerite dyke, which has previously yielded baddeleyite ID-TIMS U–Pb ages of 2610 ± 25 Ma and 1390 ± 3 Ma (Stark et al., 2018a; Stark et al., 2018b). In our data, out of 27 grains of apatites analysed for Lu—Hf ratios, only five grains preserve a primary Archean crystallization age of 2677 ± 128 Ma. The Lu—Hf ratios for the other apatite grains in this sample have large individual uncertainties and define an array with an imprecise Lu—Hf age of 991 ± 66 Ma. The trace element data plot as a linear array in the low-temperature field on the LREE vs Sr/Y biplot (Fig. 5d). There is no clear difference in trace element composition for the grains that preserve an Archean Lu—Hf age, compared to the other analysed apatite grains from this sample. Hence, the preferred interpretation is that the majority of the apatite recrystallized under low-temperature metamorphic conditions. The five Archean apatite grains dated in sample 7910–150 are interpreted to record the primary mafic emplacement age of the dyke prior to recrystallization. The imprecise Lu—Hf isochron age of 991 ± 66 Ma agrees within uncertainty with published biotite $^{40}Ar/^{39}Ar$ and Rb—Sr ages of ~1000–1100 Ma from the same locality, which are thought to represent a thermal event and thus a cooling age, or possibly a fluid flow event (Lu et al., 2015). These ages correspond to the AFO Stage I metamorphic event in the adjacent Pinjara Orogen that is constrained by metamorphic monazite U–Pb ages of 1083 ± 3 Ma and 1023 ± 9 Ma, a U–Pb apatite cooling age of 921 ± 23 Ma, and youngest detrital zircon U–Pb ages between ~1100 Ma and ~ 1023 Ma from the Northampton and Mullingarra complexes in the north of the Pinjara Orogen (Bruguier et al., 1999; Ksienzyk et al., 2012).

The apatite U–Pb data from samples SWY-29 and 7910–150 from the southwest Yilgarn Craton both record significant scatter and Neoproterozoic ages of 661 ± 17 Ma and 567 ± 12 Ma, respectively. Given the significant degree of scatter and associated high MSWD values, these ages are unlikely to record the timing of mafic magmatism and instead are attributed to open system behaviour during a subsequent Ediacaran thermal event, likely corresponding to the ~750–520 Ma Kuunga Orogeny, which occurred when Indo-Antarctica and Australo-Antarctica collided during the assembly of Gondwana (Markwitz et al., 2017; Halpin et al., 2017; Daczko et al., 2018; Mulder et al., 2019). The youngest U–Pb age obtained is consistent with ~590–560 Ma biotite Rb—Sr ages for the sheared margins of a similar NW-trending mafic dyke within the same terrane (Compston and Arriens, 1968). A number of studies (Libby et al., 1999: Libby and De Laeter, 1998; Lu et al., 2015) obtained <1000 Ma Rb—Sr biotite ages along the western margin of the SW terrane, indicating a significant late Neoprotorozoic to early Palaeozoic thermal event within the region.

This case study illustrates that dating mafic magmatism in complex hot terranes remains challenging. However, where the apatite trace elements preserve a primary mafic composition, Lu—Hf dates can confidently be used to constrain magmatic emplacement ages. When the trace element data record high-temperature or low-temperature modifications, the Lu—Hf system might record the timing of metamorphism and/or deformation. The U–Pb dates, however, record cooling ages related to the last significant regional thermal event.

6. Conclusion

This study demonstrates that apatite Lu—Hf dating is a suitable method to date the timing of magmatic crystallization of mafic rocks. Given the higher closure temperature of the apatite Lu—Hf system compared to the U–Pb system, Lu—Hf dates are more likely to preserve the timing of apatite crystallization in terranes that have undergone significant post-magmatic reworking. In such terranes, apatite U–Pb dates are often cooling ages that may have limited geological significance. Apatite trace element composition is a key monitor for potential later modification of the grain chemistry (i.e., by dissolution/reprecipitation). If secondary disturbances are detected (LREE and/or Sr depletion), apatite may have been recrystallized or the Lu—Hf system might have been disturbed by volume diffusion. In such cases, the Lu—Hf system may date the timing of deformation or metamorphism.

Author credit statement

M. Kharkongor: experimentation, data interpretation, visualization, formal analysis, manuscript drafting and editing; S. Glorie: conceptualisation, data interpretation, manuscript drafting and editing, primary supervision; J. Mulder: data interpretation, manuscript editing, supervision; C. Kirkland: conceptualisation, manuscript editing, supervision; D. Chew: conceptualisation, manuscript editing; B. Kohn: providing samples, manuscript editing; A. Simpson: manuscript editing, method development.

Declaration of Competing Interest

The authors declare that they have no known competing financial interests or personal relationships that could have appeared to influence the work reported in this paper.

Data availability

All data is included in the submission

Acknowledgements

This study was funded by a Discovery Grant from the Australian Research Council (ARC DP200101881). Sarah Gilbert is thanked for her assistance with LA-ICP-MS data collection. Klaus Mezger and an anonymous reviewer are thanked for their constructive reviews. The University of Melbourne thermochronology laboratory from which apatite separates were sourced receives support under the AuScope program of the National Collaborative Research Infrastructure Strategy (NCRIS).

Appendix A. Supplementary data

Supplementary data to this article can be found online at https://doi.org/10.1016/j.chemgeo.2023.121630.

References

Ackerman, L., et al., 2020. Petrogenesis and Lu–Hf Dating of (Ultra)Mafic Rocks from the Kutná Hora Crystalline complex: Implications for the Devonian Evolution of the Bohemian Massif. J. Petrol. 61 (8) https://doi.org/10.1093/petrology/egaa075.

Almeida, F.D., Hasui, Y., Brito Neves, B.D., Fuck, R.A., 1977. Províncias estruturais brasileiras. Simpósio de Geologia do Nordeste 8 (1977), 363–391.

Aragão, A.J.S., Gorayeb, P.S.D.S., Galarza, M.A., 2020. Magmatic and tectonic evolution of the Chaval Granite at the end of the Neoproterozoic, northwestern border of the Borborema Province. Brazilian. J. Geol. 50 (1) https://doi.org/10.1590/2317-4889202020190089.

Archanjo, C.J., Viegas, L.G., Hollanda, M.H.B., Souza, L.C., Liu, D., 2013. Timing of the HT/LP transpression in the Neoproterozoic Seridó Belt (Borborema Province, Brazil): Constraints from UPb (SHRIMP) geochronology and implications for the connections between NE Brazil and West Africa. Gondwana Res. 23 (2), 701–714. https://doi.org/10.1016/j.gr.2012.05.005.

Barfod, G.H., et al., 2002. New Lu–Hf and Pb–Pb age constraints on the earliest animal fossils. Earth Planet. Sci. Lett. 201 (1), 203–212. https://doi.org/10.1016/S0012-821X(02)00687-8.

Barfod, G.H., Otero, O., Albarède, F., 2003. Phosphate Lu–Hf geochronology. Chem. Geol. 200 (3–4), 241–253. https://doi.org/10.1016/S0009-2541(03)00202-X.

Barfod, G.H., Krogstad, E.J., Frei, R., Albarède, F., 2005. Lu-Hf and PbSL geochronology of apatites from Proterozoic terranes: A first look at Lu-Hf isotopic closure in metamorphic apatite. Geochim. Cosmochim. Acta 69 (7), 1847–1859. https://doi.org/10.1016/j.gca.2004.09.014.

Bethune, K.M., Davidson, A., 1997. Grenvillian metamorphism of the Sudbury diabase dyke-swarm; from protolith to two-pyroxene—garnet coronite. Can. Mineral. 35 (5), 1191–1220.
Black, L.P., Harris, L.B., Delor, C.P., 1992. Reworking of Archaean and early Proterozoic components during a progressive, middle Proterozoic tectonothermal event in the Albany Mobile Belt, Western Australia. Precambrian Res. 59 (1–2), 95–123. https://doi.org/10.1016/0301-9268(92)90053-Q.
Boehnke, P., Watson, E.B., Trail, D., Harrison, T.M., Schmitt, A.K., 2013. Zircon saturation re-revisited. Chem. Geol. 351, 324–334. https://doi.org/10.1016/j.chemgeo.2013.05.028.
Bruguier, O., Bosch, D., Pidgeon, R., Byrne, D., Harris, L., 1999. U-Pb chronology of the Northampton complex, Western Australia–evidence for Grenvillian sedimentation, metamorphism and deformation and geodynamic implications. Contrib. Mineral. Petrol. 136, 258–272. https://doi.org/10.1007/s004100050537.
Cassidy, K., et al., 2006. A revised geological framework for the Yilgarn Craton, Western Australia. Geol. Surv. Western Aust. Rec. 8 (8), 15.
Caxito, F.D.A., et al., 2020. Toward an integrated model of geological evolution for NE Brazil-NW Africa: the Borborema Province and its connections to the Trans-Saharan (Benino-Nigerian and Tuareg shields) and Central African orogens. Braz. J. Geol. 50 https://doi.org/10.1590/2317-4889202020190122.
Cherniak, 2000. Rare earth element diffusion in apatite. Geochim. Cosmochim. Acta 64 (22), 3871–3885. https://doi.org/10.1016/S0016-7037(00)00467-1.
Chew, D.M., Spikings, R.A., 2015. Geochronology and Thermochronology using Apatite: Time and Temperature, lower crust to surface. Elements 11 (3), 189–194. https://doi.org/10.2113/gselements.11.3.189.
Chew, D.M., Petrus, J.A., Kamber, B.S., 2014. U–Pb LA–ICPMS dating using accessory mineral standards with variable common Pb. Chem. Geol. 363 https://doi.org/10.1016/j.chemgeo.2013.11.006, 185–19.
Clark, M.D., Riller, U., 2018. 3-D kinematic restoration of the eastern Sudbury Igneous complex, Canada, and its importance for Cu-Ni-PGE sulphide exploration. Ore Geol. Rev. 101, 199–210. https://doi.org/10.1016/j.oregeorev.2018.07.019.
Clark, D., Kinny, P., Post, N., Hensen, B., 1999. Relationships between magmatism, metamorphism and deformation in the Fraser Complex, Western Australia: constraints from new SHRIMP U–Pb zircon geochronology. Aust. J. Earth Sci. 46 (6), 923–932. https://doi.org/10.1046/j.1440-0952.1999.00753.x.
Clark, D., Hensen, B., Kinny, P., 2000. Geochronological constraints for a two-stage history of the Albany–Fraser Orogen, Western Australia. Precambrian Res. 102 (3–4), 155–183. https://doi.org/10.1016/S0301-9268(00)00063-2.
Compston, W., Arriens, P., 1968. The Precambrian geochronology of Australia. Can. J. Earth Sci. 5 (3), 561–583. https://doi.org/10.1139/e68-052.
Corfu, F., Lightfoot, P., 1996. U-Pb geochronology of the sublayer environment, Sudbury Igneous complex, Ontario. Econ. Geol. 91 (7), 1263–1269. https://doi.org/10.2113/gsecongeo.91.7.1263.
Daczko, N.R., Halpin, J.A., Fitzsimons, I.C., Whittaker, J.M., 2018. A cryptic Gondwana-forming orogen located in Antarctica. Sci. Rep. 8 (1), 1–9. https://doi.org/10.1038/2Fs41598-018-26530-1.
Dantas, A.R., 2017. Petrografia e litoquímica de rochas ferríferas na região central do estado do Rio Grande do Norte (domínio do rio Piranhas-Seridó, NE da província Borborema). https://doi.org/10.11606/issn.2316-9095.v17-125622.
De Almeida, F., Hasui, Y., de Brito Neves, B., Fuck, R.A., 1981. Brazilian structural provinces: an introduction. Earth Sci. Rev. 17 (1–2), 1–29. https://doi.org/10.1016/0012-8252(81)90003-9.
Dessureau, 2003. Geochemistry of the Mafic and Felsic Norite: Implications for the Crystallization History of the Sudbury Igneous Complex, Sudbury Ontario, Laurentian University, Sudbury, Ontario (MasterThesis)152pp. https://nicholas.duke.edu/people/faculty/boudreau/9thPtSymposium/Dessureau_Abstract.pdf.
Dickin, A., Richardson, J., Crocket, J., McNutt, R., Peredery, W., 1992. Osmium isotope evidence for a crustal origin of platinum group elements in the Sudbury nickel ore, Ontario, Canada. Geochim. Cosmochim. Acta 56 (9), 3531–3537.
Dietz, R.S., 1964. Sudbury structure as an astrobleme. J. Geol. 72 (4), 412–434. https://doi.org/10.1086/626999.
Dressler, B.O., Pye, E., Naldrett, A., 1984. General geology of the Sudbury area, the geology and ore deposits of the Sudbury structure. Ontario Geol. Surv. Toronto 57–82.
Fisher, C.M., Vervoort, J.D., 2018. Using the magmatic record to constrain the growth of continental crust—the Eoarchean zircon Hf record of Greenland. Earth Planet. Sci. Lett. 488, 79–91. https://doi.org/10.1016/j.epsl.2018.01.031.
Fleet, M.E., Barnett, R.L., Morris, W.A., 1987. Prograde metamorphism of the Sudbury igneous complex. Can. Mineral. 25 (3), 499–514.
Gaál, G., Gorbatschev, R., 1987. An outline of the Precambrian evolution of the Baltic Shield. Precambrian Res. 35, 15–52. https://doi.org/10.1016/0301-9268(87)90044-1.
Galindo, A.C., 1993. Petrologia dos Granitoides Brasilianos da regiao de Caraúbas-Umarizal, oeste do Rio Grande do Norte (Ph.D. thesis).. Centro de Geociˆencias, Universidade Federal do Par_a, p. 370 http://bdtd.ibict.br/vufind/Record/UFPA_a46abcee32e1a806f4818a21e0d24144.
Galindo, A., Dall'Agnol, R., McReath, I., Lafon, J., Teixeira, N., 1995. Evolution of Brasiliano-age granitoid types in a shear-zone environment, Umarizal-Caraubas region, Rio Grande do Norte, Northeast Brazil. J. S. Am. Earth Sci. 8 (1), 79–95. https://doi.org/10.1016/0895-9811(94)00043-2.
Gehrels, G., 2011. Detrital Zircon U-Pb Geochronology: Current Methods and New Opportunities. Tect. Sediment. Basins 45–46. https://doi.org/10.1002/9781444347166.ch2.
Gillespie, J., Glorie, S., Khudoley, A., Collins, A.S., 2018. Detrital apatite U-Pb and trace element analysis as a provenance tool: Insights from the Yenisey Ridge (Siberia). Lithos 314-315, 140–155. https://doi.org/10.1016/j.lithos.2018.05.026.
Gillespie, J., et al., 2022. Lu–Hf, Sm–Nd, and U–Pb isotopic coupling and decoupling in apatite. Geochim. Cosmochim. Acta 338, 121–135. https://doi.org/10.1016/j.gca.2022.09.038.
Glorie, S., et al., 2019. Thermochronological and geochemical footprints of post-orogenic fluid alteration recorded in apatite: Implications for mineralisation in the Uzbek Tian Shan. Gondwana Res. 71, 1–15. https://doi.org/10.1016/j.gr.2019.01.011.
Glorie, S., et al., 2022. Detrital apatite Lu–Hf and U–Pb geochronology applied to the southwestern Siberian margin. Terra Nova 34 (3), 201–209. https://doi.org/10.1111/ter.12580.
Glorie, S., et al., 2023. Robust laser ablation Lu-Hf dating of apatite: an empirical evaluation. Geol. Soc. Lond., Spec. Publ. 537 (1) https://doi.org/10.1144/sp537-2022-205.
Gorbatschev, R., Bogdanova, S., 1993. Frontiers in the Baltic shield. Precambrian Res. 64 (1–4), 3–21. https://doi.org/10.1016/0301-9268(93)90066-B.
Grieve, R., Lightfoot, P., Naldrett, A., 1994. An impact model of the Sudbury structure. In: Proceedings of the Sudbury Noril'sk Symposium. Ministry of Northern Development and Mines, Ontario, pp. 119–132.
Häkli, T., 1971. Silicate nickel and its application to the exploration of nickel ores. Bull. Geol. Soc. Finl. 43 (2), 247–263. https://doi.org/10.17741/bgsf/43.2.009.
Halpin, J.A., Daczko, N.R., Kobler, M.E., Whittaker, J.M., 2017. Strike-slip tectonics during the Neoproterozoic–Cambrian assembly of East Gondwana: Evidence from a newly discovered microcontinent in the Indian Ocean (Batavia Knoll). Gondwana Res. 51, 137–148. https://doi.org/10.1016/j.gr.2017.08.002.
Helovuori, O., 1979. Geology of the Pyhasalmi ore deposit, Finland. Econ. Geol. 74 (5), 1084–1101. https://doi.org/10.2113/gsecongeo.74.5.1084.
Henrichs, I., et al., 2019. Trace element (Mn-Sr-Y-Th-REE) and U-Pb isotope systematics of metapelitic apatite during progressive greenschist-to amphibolite-facies Barrovian metamorphism. Geochem. Geophys. Geosyst. 20 (8), 4103–4129. https://doi.org/10.1029/2019GC008359.
Hermansson, T., Stephens, M.B., Corfu, F., Page, L.M., Andersson, J., 2008. Migratory tectonic switching, western Svecofennian orogen, Central Sweden: Constraints from U/Pb zircon and titanite geochronology. Precambrian Res. 161 (3–4), 250–278. https://doi.org/10.1016/j.precamres.2007.08.008.
Huhma, H., 1986. Sm-Nd, U-Pb and Pb-Pb isotopic evidence for the origin of the early Proterozoic Svecokarelian crust in Finland. Geol. Surv. Finland Bull. 337.
Ihlen, P.M., Schiellerup, H., Gautneb, H., Skår, Ø., 2014. Characterization of apatite resources in Norway and their REE potential—a review. Ore Geol. Rev. 58, 126–147. https://doi.org/10.1016/j.oregeorev.2013.11.003.
Jennings, E.S., Marschall, H., Hawkesworth, C., Storey, C., 2011. Characterization of magma from inclusions in zircon: Apatite and biotite work well, feldspar less so. Geology 39 (9), 863–866. https://doi.org/10.1130/G32037.1.
Jiang, Q., et al., 2021. 40Ar/39Ar dating of basaltic rocks and the pitfalls of plagioclase alteration. Geochim. Cosmochim. Acta 314, 334–357. https://doi.org/10.1016/j.gca.2021.08.016.
Kärki, A., Laajoki, K., 1995. An interlinked system of folds and ductile shear zones—late stage Svecokarelian deformation in the central Fennoscandian Shield, Finland. J. Struct. Geol. 17 (9), 1233–1247. https://doi.org/10.1016/0191-8141(95)00006-Y.
Kilpeläinen, T., 1998. Evolution and 3D modelling of structural and metamorphic patterns of the Palaeoproterozoic crust in the Tampere-Vammala area southern Finland. Geol. Surv. Fin. 397. https://tupa.gtk.fi/julkaisu/bulletin/bt_397.pdf. ISSN0367522X.
Kirkland, C., Wingate, M.T.D., Spaggiari, C.V., Pawley, M.J., 2012. 184374: Monzogranite, Mount Ridley; Geochronology Record 1045:Geological Survey of Western Australia (4p).
Kirkland, C.L., et al., 2018. Apatite: a U-Pb thermochronometer or geochronometer? Lithos 318-319, 143–157. https://doi.org/10.1016/j.lithos.2018.08.007.
Koistinen, T.J., 1981. Structural evolution of an early Proterozoic strata-bound Cu-Co-Zn deposit, Outokumpu, Finland. Earth Environ. Sci. Transact. R. Soc. Edinburgh 72 (2), 115–158. https://doi.org/10.1017/S0263593300009949.
Korsman, K., 1988. Tectono-metamorphic evolution of the Raahe-Ladoga zone. Geol. Surv. Fin. Bull. 343, 98 pp. https://tupa.gtk.fi/julkaisu/bulletin/bt_343.pdf.
Korsman, K., Hölttä, P., Hautala, T., Wasenius, P., 1984. Metamorphism as an indicator of evolution and structure of the crust in eastern Finland. Geol. Surv. Finl. Bull. 328, 40. https://tupa.gtk.fi/julkaisu/bulletin/bt_328.pdf.
Korsman, K., Korja, T., Pajunen, M., Virransalo, P., Group, G.S.W, 1999. The GGT/SVEKA transect: structure and evolution of the continental crust in the Paleoproterozoic Svecofennian orogen in Finland. Int. Geol. Rev. 41 (4), 287–333. https://doi.org/10.1080/00206819909465144.
Krogh, T.E., et al., 1984. Precise U-Pb Zircon and Baddeleyite Ages for the Sudbury Area, the Geology and Ore Deposits of the Sudbury Structure. Ontario Geological Survey Toronto, Ont., Canada, pp. 431–446.
Ksienzyk, A.K., et al., 2012. U–Pb ages of metamorphic monazite and detrital zircon from the Northampton Complex: evidence of two orogenic cycles in Western Australia. Precambrian Res. 198, 37–50. https://doi.org/10.1016/j.precamres.2011.12.011.
Lahtinen, R., 1994. Crustal evolution of the Svecofennian and Karelian domains during 2.1-1.79 Ga, with special emphasis on the geochemistry and origin of 1.93-1.91 Ga gneissic tonalites and associated supracrustal rocks in the Rautalampi area, central Finland. Geol. Surv. Fin. Bull. 378, 130. https://tupa.gtk.fi/julkaisu/bulletin/bt_378.pdf.
Larsson, D., Söderlund, U., 2005. Lu–Hf apatite geochronology of mafic cumulates: an example from a Fe–Ti mineralization at Smålands Taberg, southern Sweden. Chem. Geol. 224 (4), 201–211. https://doi.org/10.1016/j.chemgeo.2005.07.007.
Lee, J.K., Williams, I.S., Ellis, D.J., 1997. Pb, U and Th diffusion in natural zircon. Nature 390 (6656), 159–162. https://doi.org/10.1038/36554.

Lehtinen, M., Nurmi, P.A., Ramo, O., 2005. Precambrian Geology of Finland. Elsevier. https://www.elsevier.com/books/precambrian-geology-of-finland/lehtinen/978-0-444-51421-9.
Leterrier, J., Jardim de Sá, E., Bertrand, J.-M., Pin, C., 1994. Ages U-Pb sur Zircon de granitoïdes brasilianos de la ceinture de Seridó (Province Borborema, NE Brésil). Comptes rendus de l'Académie des sciences. Série 2. Sciences de la terre et des planètes 318 (11), 1505–1511. http://pascal-francis.inist.fr/vibad/index.php?action=getRecordDetail&idt=4270762.
Lethtovaara, 1976. Apatite Fission Track Dating of Finnish Pre-Cambrian Intrusives. Institute of Geology and Mineralogy, Univeristy of Turku, Helsinki. http://pascal-francis.inist.fr/vibad/index.php?action=getRecordDetail&idt=PASCALGEODEBRGM7620269842.
Li, Y., Vermeesch, P., 2021. Inverse isochron regression for Re–Os, K–Ca and other chronometers. Geochronology 3 (2), 415–420. https://doi.org/10.5194/gchron-2021-7.
Libby, W., De Laeter, J., 1998. Biotite Rb-Sr age evidence for early Palaeozoic tectonism along the cratonic margin in southwestern Australia. Aust. J. Earth Sci. 45 (4), 623–632. https://doi.org/10.1080/08120099808728417.
Libby, W., De Laeter, J., Armstrong, R., 1999. Proterozoic biotite Rb–Sr dates in the northwestern part of the Yilgarn Craton, Western Australia. Aust. J. Earth Sci. 46 (6), 851–860. https://doi.org/10.1046/j.1440-0952.1999.00749.x.
Liebmann, J., et al., 2023. Albany K-Feldspar: A New Pb Isotope Reference Material. Geostand. Geoanal. Res. https://doi.org/10.1111/ggr.12487.
Lightfoot, P.C., Doherty, W., 2001. Chemical evolution and origin of nickel sulfide mineralization in the Sudbury Igneous complex, Ontario, Canada. Econ. Geol. 96 (8), 1855–1875. https://doi.org/10.2113/96.8.1855.
Lightfoot, P.C., Keays, R.R., Morrison, G.G., Bite, A., Farrell, K.P., 1997. Geochemical relationships in the Sudbury igneous complex; origin of the main mass and offset dikes. Econ. Geol. 92 (3), 289–307. https://doi.org/10.2113/gsecongeo.92.3.289.
Lorencak, M., Kohn, B.P., Osadetz, K.G., Gleadow, A.J.W., 2004. Combined apatite fission track and (U–Th)/he thermochronometry in a slowly cooled terrane: results from a 3440-m-deep drill hole in the southern Canadian Shield. Earth Planet. Sci. Lett. 227 (1–2), 87–104. https://doi.org/10.1016/j.epsl.2004.08.015.
Lu, S., Phillips, D., Kohn, B., Gleadow, A., Matchan, E., 2015. Thermotectonic evolution of the western margin of the Yilgarn craton, Western Australia: New insights from 40Ar/39Ar analysis of muscovite and biotite. Precambrian Res. 270, 139–154. https://doi.org/10.1016/j.precamres.2015.09.014.
Mäkinen, J., 1987. Geochemical Characteristics of Svecokarelidic Mafic-Ultramafic Intrusions Associated with Ni-cu Occurrences in Finland. University of Turku, Institute of Geology and Mineralogy, Finland ((PhD thesis), Bulletin 342,90p).
Mäkinen, J., Makkonen, H.V., 2004. Petrology and structure of the Palaeoproterozoic (1.9 Ga) Rytky nickel sulphide deposit, Central Finland: a comparison with the Kotalahti nickel deposit. Mineral. Deposita 39, 405–421. https://doi.org/10.1007/s00126-004-0413-4.
Makkonen, H.V., 2005. Intrusion model for Svecofennian (1.9 Ga) mafic-ultramafic intrusions in Finland. In: Special Paper-Geological Survey of Finland, 38, p. 11.
Makkonen, H.V., Mäkinen, J., Kontoniemi, O., 2008. Geochemical discrimination between barren and mineralized intrusions in the Svecofennian (1.9 Ga) Kotalahti Nickel Belt, Finland. Ore Geol. Rev. 33 (1), 101–114. https://doi.org/10.1016/j.oregeorev.2006.05.011.
Markwitz, V., Kirkland, C.L., Evans, N.J., 2017. Early Cambrian metamorphic zircon in the northern Pinjarra Orogen: Implications for the structure of the West Australian Craton margin. Lithosphere 9 (1), 3–13. https://doi.org/10.1130/l569.1.
McArthur, J., 1985. Francolite geochemistry—compositional controls during formation, diagenesis, metamorphism, and weathering. Geochim. Cosmochim. Acta 49 (1), 23–35. https://doi.org/10.1016/0016-7037(85)90188-7.
McReath, I., Galindo, A., Dall'Agnol, R., 2002. The Umarizal igneous association, Borborema Province, NE Brazil: implications for the genesis of A-type granites. Gondwana Res. 5 (2), 339–353. https://doi.org/10.1016/S1342-937X(05)70727-9.
Medeiros, V., et al., 2021. The Rio Piranhas-Seridó Domain, Borborema Province, Northeastern Brazil: Review of geological-geochronological data and implications for stratigraphy and crustal evolution. J. Geol. Surv. Brazil 4 (3), 179–207. https://doi.org/10.29396/jgsb.2021.v4.n3.1.
Milkereit, B., Green, A., 1992. Deep geometry of the Sudbury structure from seismic reflection profiling. Geology 20 (9), 807–811. https://doi.org/10.1130/0091-7613(1992)020/3C0807:DGOTSS%3E2.3.CO;2.
Mulder, J.A., et al., 2019. A Multiproxy provenance approach to uncovering the assembly of East Gondwana in Antarctica. Geology 47 (7), 645–649. https://doi.org/10.1130/g45952.1.
Myers, J.S., 1993. Precambrian history of the West Australian craton and adjacent orogens. Annu. Rev. Earth Planet. Sci. 21 (1), 453–485. https://doi.org/10.1146/annurev.ea.21.050193.002321.
Myers, J.S., 1995. Geology of the Esperance 1:1 000 000 Sheet: Geological Survey of Western Australia, 1:1 000 000 Gelogical Series Explanatory Notes (10p).
Naldrett, A., Bray, J., Gasparrini, E., Podolsky, T., Rucklidge, J., 1970. Cryptic variation and the petrology of the Sudbury nickel irruptive. Econ. Geol. 65 (2), 122–155. https://doi.org/10.2113/gsecongeo.65.2.122.
Nascimento Souza, Z.S.D., Oliveira, E.P.D., 2022. U-Pb zircon age of Ediacaran Umarizal Granite Suite and emplacement mechanism with high-T hornfels generation in Jucurutu Formation, Borborema Province, NE, Brazil. Braz. J. Geol. 52 https://doi.org/10.1590/2317-4889202220200129.
Nascimento, M.A.L., Galindo, A.C., de Medeiros, V.C., 2015. Ediacaran to Cambrian magmatic suites in the Rio Grande do Norte domain, extreme Northeastern Borborema Province (NE of Brazil): current knowledge. J. S. Am. Earth Sci. 58, 281–299. https://doi.org/10.1016/j.jsames.2014.09.008.
Nebel, O., Morel, M.L., Vroon, P.Z., 2009. Isotope dilution determinations of Lu, Hf, Zr, Ta and W, and Hf isotope compositions of NIST SRM 610 and 612 glass wafers. Geostand. Geoanal. Res. 33 (4), 487–499. https://doi.org/10.1111/j.1751-908X.2009.00032.x.
Nelson, D., Myers, J., Nutman, A., 1995. Chronology and evolution of the Middle Proterozoic Albany-Fraser Orogen, Western Australia. Aust. J. Earth Sci. 42 (5), 481–495. https://doi.org/10.1080/08120099508728218.
Neves, S.P., 2003. Proterozoic history of the Borborema province (NE Brazil): Correlations with neighboring cratons and Pan-African belts and implications for the evolution of western Gondwana. Tectonics 22 (4), n/a-n/a. https://doi.org/10.1029/2001tc001352.
Neves, B.B.D.B., Fuck, R.A., Pimentel, M.M., 2014. The Brasiliano collage in South America: a review. Braz. J. Geol. 44, 493–518. https://doi.org/10.5327/Z2317-4889201400030010.
Norris, A., Danyushevsky, L., 2018. Towards Estimating the Complete Uncertainty Budget of Quantified Results Measured by LA-ICP-MS. Goldschmidt: Boston, MA, USA.
O'Sullivan, G.J., Chew, D.M., Samson, S.D., 2016. Detecting magma-poor orogens in the detrital record. Geology 44 (10), 871–874. https://doi.org/10.1130/g38245.1.
O'Sullivan, G., Chew, D., Kenny, G., Henrichs, I., Mulligan, D., 2020. The trace element composition of apatite and its application to detrital provenance studies. Earth Sci. Rev. 201 https://doi.org/10.1016/j.earscirev.2019.103044.
Palosaari, V., Sokta, P., 1991. PARIKKALAN Ni-Cu-MALMIN LABORATORIO VAAHDOTUSTUTKIMUS. Geoanalyyttinenlaboratorio,075/Parikkala,Ni,Cu/VIP, PMS.1991,19p. https://tupa.gtk.fi/raportti/arkisto/075_parikkala_ni_cu_vip_pms_1991.pdf.
Patchett, J., Kouvo, O., 1986. Origin of continental crust of 1.9-1.7 Ga age: Nd isotopes and U-Pb zircon ages in the Svecokarelian terrain of South Finland. Contrib. Mineral. Petrol. 92, 1–12.
Peltonen, 2005. Svecofennian mafic-ultramafic intrusions. In: Precambrian Geology of Finland, Chapter 9, pp. 407–442. https://doi.org/10.1016/S0166-2635(05)80010-6.
Pesonen, L.J., 1972. On petrophysical and paleomagnetic investigations of the gabbros of the Pohjanmaa region. Middle-West Finland. NUM. 0260, P. 1 A 27http://pascalfrancis.inist.fr/vibad/index.php?action=getRecordDetail&idt=PASCALGEODEBRGM732242162.
Petrus, J.A., Kenny, G.G., Ayer, J.A., Lightfoot, P.C., Kamber, B.S., 2015. Uranium–lead zircon systematics in the Sudbury impact crater-fill: implications for target lithologies and crater evolution. J. Geol. Soc. 173 (1), 59–75. https://doi.org/10.1144/jgs2014-056.
Piccoli, P.M., Candela, P.A., 2002. Apatite in Igneous Systems. Rev. Mineral. Geochem. 48 (1), 255–292. https://doi.org/10.2138/rmg.2002.48.6.
Pidgeon, R., 1990. Timing of plutonism in the Proterozoic Albany mobile belt, southwestern Australia. Precambrian Res. 47 (3–4), 157–167. https://doi.org/10.1016/0301-9268(90)90036-P.
Pochon, A., et al., 2016. U-Pb LA-ICP-MS dating of apatite in mafic rocks: evidence for a major magmatic event at the Devonian-Carboniferous boundary in the Armorican Massif (France). Am. Mineral. 101 (11), 2430–2442. https://doi.org/10.2138/am-2016-5736.
Puetz, S.J., Spencer, C.J., 2023. Evaluating U-Pb accuracy and precision by comparing zircon ages from 12 standards using TIMS and LA-ICP-MS methods. Geosyst. Geoenviron. 2 (2) https://doi.org/10.1016/j.geogeo.2022.100177.
Puetz, S.J., Spencer, C.J., Ganade, C.E., 2021. Analyses from a validated global UPb detrital zircon database: Enhanced methods for filtering discordant UPb zircon analyses and optimizing crystallization age estimates. Earth Sci. Rev. 220, 103745 https://doi.org/10.1016/j.earscirev.2021.103745.
Sá, J., et al., 2013. Dados isotópicos U-Pb e Sm-Nd em granitos ediacaranos no oeste do Rio Grande do Norte. In: Proceeding of the 25th Symposium Geology of Northeastern, Abstract, p. 521e522.
Salli, I., 1964. The Structure and Stratigraphy of the Ylivieska-Himanka Schist Area. Finland, Valtioneuvoston kirjapaino.
Schmidt, A., Pourteau, A., Candan, O., Oberhänsli, R., 2015. Lu–Hf geochronology on cm-sized garnets using microsampling: New constraints on garnet growth rates and duration of metamorphism during continental collision (Menderes Massif, Turkey). Earth Planet. Sci. Lett. 432, 24–35. https://doi.org/10.1016/j.epsl.2015.09.015.
Schoene, B., Bowring, S.A., 2006. U–Pb systematics of the McClure Mountain syenite: thermochronological constraints on the age of the 40Ar/39Ar standard MMhb. Contrib. Mineral. Petrol. 151 (5), 615–630. https://doi.org/10.1007/s00410-006-0077-4.
Simpson, A., et al., 2021. In-situ Lu Hf geochronology of garnet, apatite and xenotime by LA ICP MS/MS. Chem. Geol. 577 https://doi.org/10.1016/j.chemgeo.2021.120299.
Smithies, R.H., Spaggiari, C.V., Kirkland, C.L., WD, M., 2014. Geochemistry and petrogenesis of igneous rocks in the Albany–Fraser Orogen: Geological Survey of Western Australia. Record 2014 (6), 12p.
Söderlund, U., et al., 2010. Towards a complete magmatic barcode for the Zimbabwe craton: Baddeleyite U–Pb dating of regional dolerite dyke swarms and sill complexes. Precambrian Res. 183 (3), 388–398. https://doi.org/10.1016/j.precamres.2009.11.001.
Souza de, Z.S., et al., 2006. Electron microprobe dating of monazite from high-T shear zones in the São José de Campestre Massif, NE Brazil. Gondwana Res. 9 (4), 441–455. https://doi.org/10.1016/j.gr.2005.11.008.
Spaggiari, C.V., Barquero-Molina, M., Tyler, I.M., Wingate, M., 2009. Interpreted Bedrock Geology of the South Yilganr and Central Albany-Fraser Orogen, Western Australia, Record 2009/10, 90p. Geological Survey of Western Australia.
Spaggiari, C.V., Korsch, R.J., Doublier, M.P., Clark, D.J., Dentith, M.C., Gessner, K., MG Doyle, I.T., Kennett, B.L.N., Costelloe, R.D., Fomin, T., Holzschuh, J., Occhipinti, S. A., Korsch, R.J., Doublier, M.P., Clark, D.J., Dentith, M.C., Gessner, K., MG Doyle, I.

T., Kennett, B.L.N., Costelloe, R.D., Fomin, T., Holzschuh, J., 2014. Interpretation of Albany–Fraser seismic lines12GA-AF1, 12GA-AF2 and 12GA-AF3:implications for crustal architecture; Geological Survey of Western Australia, Record 2014/6 (24 p).

Spear, F.S., Pyle, J.M., 2002. Apatite, Monazite, and Xenotime in Metamorphic Rocks. Rev. Mineral. Geochem. 48 (1), 293–335. https://doi.org/10.2138/rmg.2002.48.7.

Stacey, JS T., 1975. and 1JD Kramers. "Approximation of terrestrial lead isotope evolution by a two-stage model. Earth and planetary science letters 26 (2), 207–221.

Stark, J.C., et al., 2018a. 1.39 Ga mafic dyke swarm in southwestern Yilgarn Craton marks Nuna to Rodinia transition in the West Australian Craton. Precambrian Res. 316, 291–304. https://doi.org/10.1016/j.precamres.2018.08.014.

Stark, J.C., et al., 2018b. First evidence of Archean mafic dykes at 2.62 Ga in the Yilgarn Craton, Western Australia: Links to cratonisation and the Zimbabwe Craton. Precambrian Res. 317, 1–13. https://doi.org/10.1016/j.precamres.2018.08.004.

Stephens, M.B., Andersson, J., 2015. Migmatization related to mafic underplating and intra-or back-arc spreading above a subduction boundary in a 2.0–1.8 Ga accretionary orogen, Sweden. Precambrian Res. 264, 235–257. https://doi.org/10.1016/j.precamres.2015.04.019.

Therriault, A.M., Fowler, A.D., Grieve, R.A., 2002. The Sudbury Igneous complex: A Differentiated Impact Melt Sheet. Econ. Geol. 97, 1521–1540. https://doi.org/10.2113/gsecongeo.97.7.1521.

Thompson, J., et al., 2016. Matrix effects in Pb/U measurements during LA-ICP-MS analysis of the mineral apatite. J. Anal. At. Spectrom. 31 (6), 1206–1215. https://doi.org/10.1039/c6ja00048g.

Thomson, S.N., Gehrels, G.E., Ruiz, J., Buchwaldt, R., 2012. Routine low-damage apatite U-Pb dating using laser ablation–multicollector–ICPMS. Geochem. Geophys. Geosyst. 13 (2) https://doi.org/10.1029/2011GC003928.

Vaasjoki, M., Sakko, M., 1988. The Evolution of the Raahe-Ladoga Zone in Finland: Isotopic constraints, Geological Survey of Finland, Finland. Bulletin 343. https://tupa.gtk.fi/julkaisu/bulletin/bt_343_pages_007_032.pdf.

Van Schmus, W.R., de Brito Neves, B., Hackspacher, P., Babinski, M., 1995. UPb and SmNd geochronologic studies of the eastern Borborema Province, Northeastern Brazil: initial conclusions. J. S. Am. Earth Sci. 8 (3–4), 267–288. https://doi.org/10.1016/0895-9811(95)00013-6.

Vermeesch, P., 2018. IsoplotR: A free and open toolbox for geochronology. Geosci. Front. 9 (5), 1479–1493. https://doi.org/10.1016/j.gsf.2018.04.001.

Vervoort, J., 2014. Lu-Hf Dating: the Lu-Hf Isotope System. Encyclop. Scientific Dating Meth. 1–20. https://doi.org/10.1007/978-94-007-6326-5_46-1.

Ware, B., Jourdan, F., 2018. 40Ar/39Ar geochronology of terrestrial pyroxene. Geochim. Cosmochim. Acta 230, 112–136. https://doi.org/10.1016/j.gca.2018.04.002.

Webster, J.D., Piccoli, P.M., 2015. Magmatic apatite: A powerful, yet deceptive, mineral. Elements 11 (3), 177–182. https://doi.org/10.2113/gselements.11.3.177.

Wilde, S., Middleton, M., Evans, B., 1996. Terrane accretion in the southwestern Yilgarn Craton: evidence from a deep seismic crustal profile. Precambrian Res. 78 (1–3), 179–196. https://doi.org/10.1016/0301-9268(95)00077-1.

Wingate, M., Compston, W., 2000. Crystal orientation effects during ion microprobe U–Pb analysis of baddeleyite. Chem. Geol. 168 (1–2), 75–97. https://doi.org/10.1016/S0009-2541(00)00184-4.

Wingate, M., Fielding, I.O.H., Lu, Y., Ivanic, T.J., 2021. 203747: pegmatitic leucogabbro, Julimar prospect; Geochronology Record1784: Geological Survey of Western Australia (5p).

Woodard, J., et al., 2017. Zircon and monazite geochronology of deformation in the Pielavesi Shear Zone, Finland: multistage evolution of the Archaean–Proterozoic boundary in the Fennoscandian Shield. J. Geol. Soc. 174 (2), 255–267. https://doi.org/10.1144/jgs2016-020.

Zaher, M.A., Pirttijärvi, M., Korja, T., 2017. Geophysical studies of the Raahe-Ladoga Shear complex in the Iisalmi area of Finland. Geophysica 52 (2), 43–67.